Article

# Specific regulation of BACH1 by the hotspot mutant p53[R175H] reveals a distinct gain-of-function mechanism

🔴 Check for updates

Zhenyi Su[1,2], Ning Kon[1,2], Jingjie Yi[1,2], Haiqing Zhao [3], Wanwei Zhang [4], Qiaosi Tang[2], Huan Li[1,2], Hiroki Kobayashi[5], Zhiming Li [1,2], Shoufu Duan [1,2], Yanqing Liu[1,2], Kenneth P. Olive[2,5], Zhiguo Zhang [1,2], Barry Honig[3], James J. Manfredi [6], Anil K. Rustgi[2] & Wei Gu [1,2] ✉

Although the gain of function (GOF) of p53 mutants is well recognized, it remains unclear whether different p53 mutants share the same cofactors to induce GOFs. In a proteomic screen, we identified BACH1 as a cellular factor that recognizes the p53 DNA-binding domain depending on its mutation status. BACH1 strongly interacts with p53[R175H] but fails to effectively bind wild-type p53 or other hotspot mutants in vivo for functional regulation. Notably, p53[R175H] acts as a repressor for ferroptosis by abrogating BACH1-mediated downregulation of SLC7A11 to enhance tumor growth; conversely, p53[R175H] promotes BACH1-dependent tumor metastasis by upregulating expression of pro-metastatic targets. Mechanistically, p53[R175H]-mediated bidirectional regulation of BACH1 function is dependent on its ability to recruit the histone demethylase LSD2 to target promoters and differentially modulate transcription. These data demonstrate that BACH1 acts as a unique partner for p53[R175H] in executing its specific GOFs and suggest that different p53 mutants induce their GOFs through distinct mechanisms.

TP53 (p53) is the most commonly mutated gene in human cancers and p53 missense mutations are present in more than 40% of all human tumors[1–3]. Most p53 mutations are located within the DNA-binding domain, including hotspot mutations R175H, R248W, R273H, G245S, R249S and R282W. There are mainly two forms of p53 mutants: conformational mutants, such as R175H and G245S, which change the structure of the DNA-binding domain and contact mutants, such as R248W and R273H, which impair the binding of mutant p53 to DNA[4]. As a result, both types of p53 mutants are defective in DNA binding

and lose their tumor-suppressor functions[5]. In addition to loss of the wild-type p53 function, some missense substitutions, particularly 'hotspot' mutations, enable its mutant forms to gain a selective advantage during tumor development including enhanced oncogenic activity and increased metastatic potential[4,6]. It is believed that the major mechanism of the GOF of these mutants acts through interactions with other cellular factors to gain new properties, independent of wild-type p53 function. Indeed, a number of cellular proteins have been proposed as mediators of GOFs by interacting with mutant p53 (refs. [7–16]).

[1]Institute for Cancer Genetics, and Department of Pathology and Cell Biology, Vagelos College of Physicians & Surgeons, Columbia University, New York, NY, USA. [2]Herbert Irving Comprehensive Cancer Center, Vagelos College of Physicians & Surgeons, Columbia University, New York, NY, USA. [3]Departments of Biochemistry and Molecular Biophysics, Systems Biology, and Medical Sciences in Medicine, Zuckerman Institute Columbia University, New York, NY, USA. [4]Department of Microbiology and Immunology, Vagelos College of Physicians and Surgeons, Columbia University, New York, NY, USA. [5]Division of Digestive and Liver Diseases, Department of Medicine, Columbia University Irving Medical Center, New York, NY, USA. [6]Department of Oncological Sciences, Icahn School of Medicine at Mount Sinai, New York, NY, USA. ✉e-mail: wg8@cumc.columbia.edu

Notably, accumulating evidence indicates that mice carrying different mutant p53 displayed varied survival time, tumor spectrum and metastatic potential[17–19] and patients with different *p53* mutations showed different phenotypes[20], suggesting distinct mutant p53 may have their specific signaling pathways to execute specific GOFs in vivo. Nevertheless, it remains unclear whether each p53 mutant has its specific binding partner required for its specific GOFs.

The BTB and CNC homology 1 (BACH1) is a heme dependent transcriptional factor, which was reported to serve as an important factor in the physiological regulation of oxidative stress and tumor metastasis[21–29]. Through biochemical purification, we identified BACH1 as a major cellular factor specifically recognized by p53[R175H] but not by either wild-type p53 or other hotspot p53 mutants. By using two different tumor mouse models, respectively, we found that the BACH1-p53[R175H] interaction are critical for both primary tumor growth and lung metastasis in vivo. Our study provides the evidence that the tumor growth and metastasis activities of GOFs may act through different mechanisms and also reveals a new model about how different p53 mutants execute their GOFs differently.

## Results

### BACH1 specifically interacts with p53[R175H]

To elucidate the precise mechanism by which p53 missense mutants execute their GOFs in vivo, we used a proteomic screen to identify any protein that recognizes the p53 DNA-binding domain (DBD) in a manner dependent on its mutation status. To do so, we first purified the potential binding proteins associated with the p53 DBD through multi-step affinity chromatography from a SFB-p53 H1299 stable cell line (Extended Data Fig. 1a)[30,31]. The affinity-purified SFB-p53 interacting proteins were detected by liquid chromatography mass spectrometry/mass spectrometry (LC–MS/MS) and revealed a few cellular proteins that have been reported to interact with the DBD of p53, such as TP53BP1, USP28 and Sirt1 (refs.[32–34]). Notably, we also identified BACH1 from the same complex (Extended Data Fig. 1b,c). We then examined the interactions between BACH1 and p53 by coexpression in *p53*-null H1299 cells. We failed to detect any obvious interaction between BACH1 and the full-length wild-type p53 (Fig. 1c). Moreover, the hotspot mutant p53[R175H] showed a very strong interaction with BACH1, whereas other hotspot mutants failed to do so (Fig. 1c,d), suggesting that BACH1 interacts with p53[R175H] in a specific fashion. Next, we measured the binding affinity between BACH1 and different domains of p53-R175H (Fig. 1e). Indeed, the p53 DBD-R175H (amino acid (aa) 100–300) alone is responsible for the interaction with BACH1 (Fig. 1e). We further found that BACH1 strongly interacts with the DBD of p53-R175H but weakly interacts with the DBD of wild-type p53 or other p53 hot mutants, including R248W, R273H, G245S, R249S and R282W (Extended Data Fig. 1d). By using immunoprecipitation (IP) assay, we observed that p53[R175H] interacted with the C-domain of BACH1 (Fig. 1f).

To evaluate this binding under more physiological conditions, we first made a H1299 cell line stably expressing SFB-p53[R175H] and performed double co-immunoprecipitation assays for SFB-p53[R175H]. As shown in Fig. 1g, endogenous BACH1 can be co-precipitated with SFB-p53[R175H]. Moreover, we conducted the co-immunoprecipitation assay in native p53[R175H] expressing cancer cells such as the human tongue squamous cell carcinoma cell line Cal-33 and the human liver bile duct carcinoma HuCCT1 cell line. Western blot analysis revealed that endogenous BACH1 co-precipitated with endogenous p53[R175H] with the anti-p53 specific antibody but not with the IgG control (Fig. 1h,i); conversely, endogenous p53[R175H] co-precipitated with endogenous BACH1 with the anti-BACH1 specific antibody but not with the IgG control (Extended Data Fig. 1e). Similar results were obtained in p53[R172H]-expressing sarcoma cells derived from *p53*[R172H/R172H] mice (Fig. 1j). By contrast, BACH1 was not detected in the p53-associated protein complexes in either human osteosarcoma U2OS cell line or human colorectal cancer HCT116 cell lines, both of which express wild-type p53 (Fig. 1k,l). To validate further the specific interaction between BACH1 and p53[R175H], we tested whether endogenous BACH1 interacts with endogenous p53 in other native human cancer cell lines expressing p53[R273H], p53[R249S], p53[R280K], p53[E285K] and p53[L194F], respectively. None of these mutant p53 was able to interact with BACH1 in vivo (Fig. 1m–p and Extended Data Fig. 1f). To further understand the specific interaction, we identified the essential minimal region of p53 that interacts with BACH1. Western blot analysis revealed that BACH1 strongly binds SFB-p53 (amino acid (aa) 98–180-R175H), but fails to bind with SFB-p53 (aa 1–160) (Extended Data Fig. 1g), suggesting that the region containing aa 161–180 is essential for BACH1 binding. Indeed, loss of this region p53 (Δ161–180) completely abrogated the interaction between full-length p53[R175H] and BACH1 (Extended Data Fig. 1h). These data suggest the region between aa 161–180 of p53[R175H], where R175H is located, is mostly likely the docking site for BACH1 binding.

### p53[R175H] is able to suppress BACH1-mediated ferroptosis

We and others have showed that wild-type p53 sensitizes cells to ferroptotic cell death by inhibiting the *SLC7A11* gene transcription[35,36]. Notably, it has been reported that BACH1, like wild-type p53, is capable to repress the expression of SLC7A11 in mouse cells[26]. Indeed, both BACH1 knockdown and chromatin immunoprecipitation (ChIP) assays validated the premise that BACH1 mediates repression of SLC7A11 expression in human cancer cells (Fig. 2a,b). As p53[R175H] interacts with BACH1, we examined whether p53[R175H] modulates BACH1-dependent transcriptional activity. As shown in Fig. 2c, wild-type p53 expression repressed the SLC7A11 transcription; however, expression of p53[R175H] induced modest activation of SLC7A11 expression. Notably, BACH1 alone also repressed SLC7A11 expression but coexpression of p53[R175H] with BACH1 was able to abrogate BACH1-mediated repression of the SLC7A11 expression (Fig. 2c). To further validate that p53[R175H]-mediated effect on SLC7A11 expression acts through BACH1, we performed the similar experiments by using a SLC7A11 reporter gene with the mutated BACH1 motif. As expected, BACH1 failed to repress SLC7A11 transcription (Extended Data Fig. 2a,b); more notably, no obvious effect on the SLC7A11 transcription (the mutant construct) was observed in the presence of p53[R175H] expression. Next, we examined the effects on SLC7A11 levels by knockdown of endogenous p53[R175H] in native p53[R175H] expressing human cancer cells. As expected, SLC7A11 levels were dramatically upregulated in *p53*-null HCT116 cells as wild-type p53 is able to repress SLC7A11 expression (Fig. 2d). In contrast, knockdown of p53[R175H] in

**Fig. 1 | Identification of BACH1 as a specific binding partner of p53[R175H].**
**a,b** Diagram of p53 (**a**) and BACH1 (**b**) structure and truncated derivatives. TAD, transactivation domain; PRD, proline-rich domain; DBD, DNA-binding domain; TD, tetramerization domain; CTD, C-terminal domain; BTB, broad-complex, tramtrack and bric-a-brac; bZip, basic leucine zipper; CLS, cytoplasmic localization signal. **c**, Co-IP of SFB-tagged BACH1 with untagged p53, Flag-p53[R175H], Flag-p53[R248W] and Flag-p53[R273H] in H1299 cells. SFB, S-protein-Flag-SBP. SBP, Streptavidin-binding peptide. **d**, Co-IP of Flag-HA (FH)-tagged BACH1 with SFB-tagged p53[R175H], p53[G245S], p53[R249S] and p53[R282W] in H1299 cells. **e**, Co-IP of SFB-tagged p53[R175H] and its truncated domains (N, DBD-R175H and C) with FH-BACH1. FL, full-length wild-type p53; N, N terminus; C, C terminus; **f**, Co-IP of SFB-tagged BACH1 and its truncated domains (N, M and C) with p53[R175H]. **g**, Double co-IP of SFB-p53[R175H] and endogenous BACH1 in H1299 cell line stably expressing SFB-p53[R175H] protein. First round: streptavidin beads; second round: S-protein beads. **h–j**, Endogenous co-IP of p53 and BACH1 in p53[R175H] native cell lines Cal-33 (**h**) and HuCCT1(**i**) and *p53*[R172H/R172H] mice derived sarcoma cells (**j**). Ab, antibody. **k,l**, Endogenous co-IP of p53 and BACH1 in wild-type p53 cell lines U2OS (**k**) and HCT116 (**l**). **m–p**, Endogenous co-IP of p53 and BACH1 in mutant p53 cell lines MDA-MB-468 (**m**, p53[R273H]), BT-549 (**n**, p53[R249S]), T-47D (**o**, p53[L194F]) and BT-474 (**p**, p53[E285K]). Western blot experiments above (**c–p**) were repeated three times with similar results and representative images are shown.
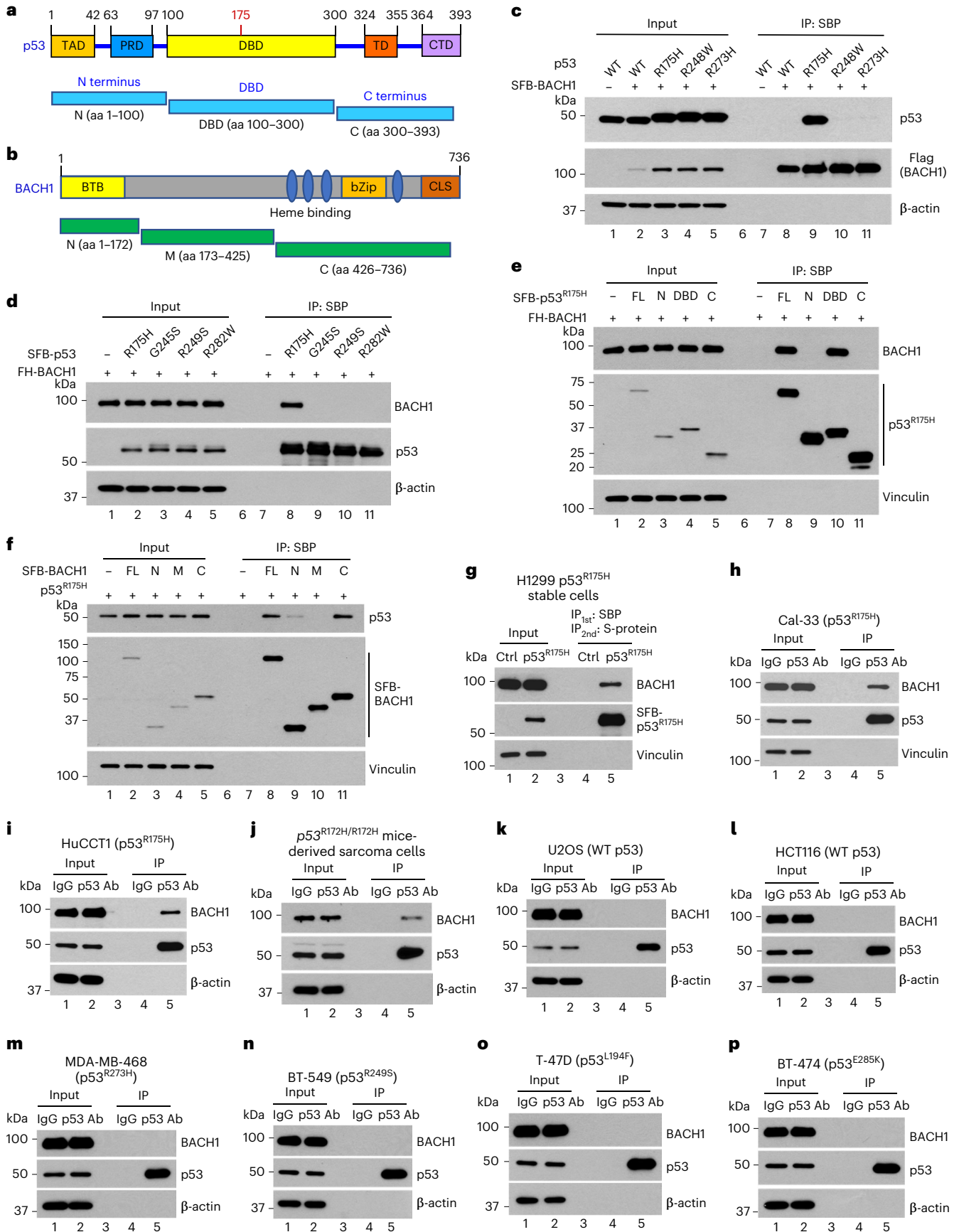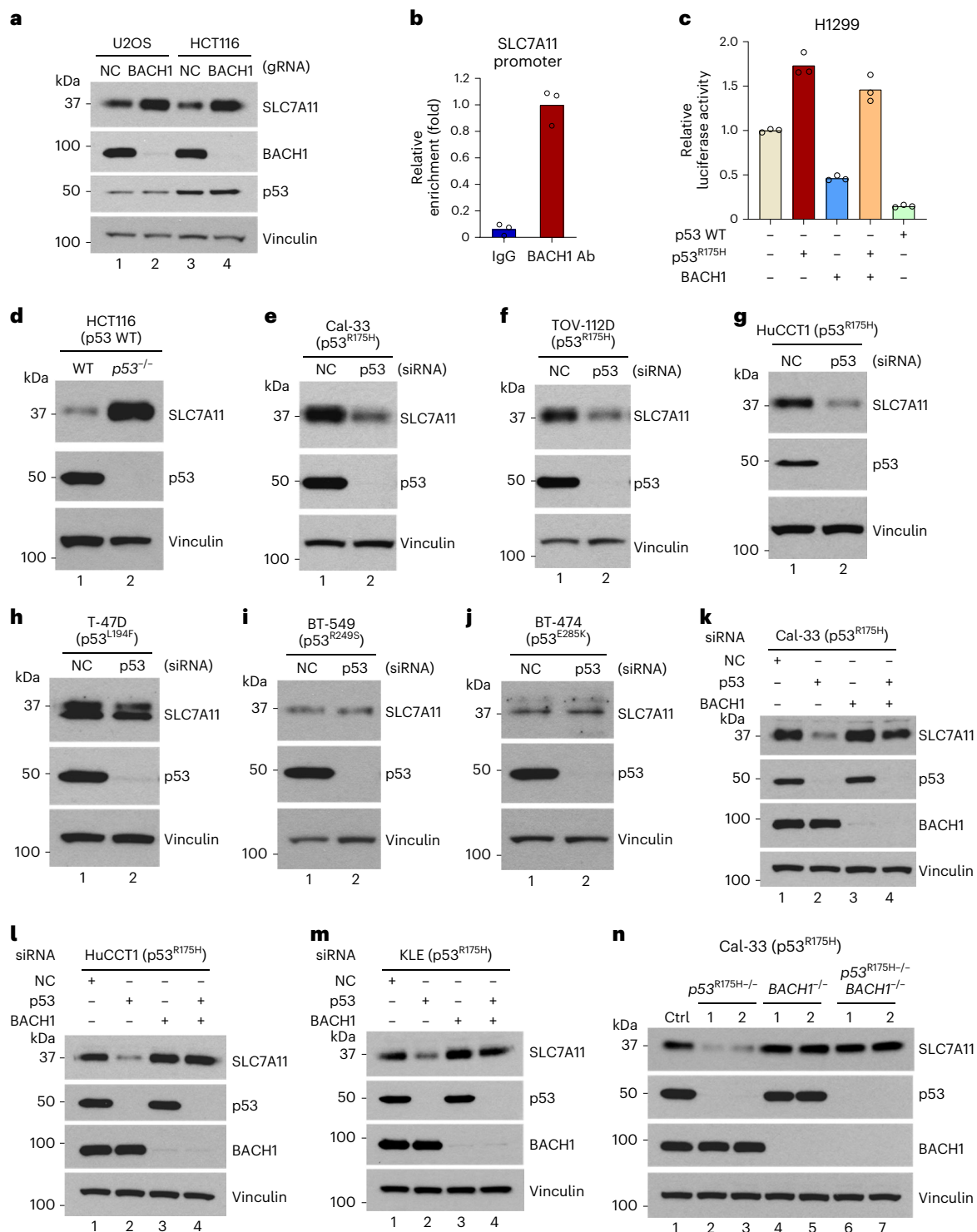
**Fig. 2 | BACH1-mediated transcriptional repression of SLC7A11 is abrogated by p53^R175H. a**, Western blot analysis of SLC7A11 expression in U2OS and HCT116 cells transfected with negative control (NC) or BACH1 gRNAs for 48 h. **b**, ChIP analysis of the recruitment of BACH1 to SLC7A11 promoter (−128 to −114) in Cal-33 cells. $n = 3$ technical replicates. The experiment was repeated three times with similar results. **c**, Dual-luciferase reporter assay for SLC7A11 transcription in H1299 cells transfected with control (Ctrl), p53 wild-type (WT), p53^R175H, BACH1, p53 WT + BACH1 or p53^R175H + BACH1 plasmids ($n = 3$ technical cell culture replicates). The experiment was repeated three times with similar results. **d**, Western blot analysis of SLC7A11 expression in HCT116 p53 WT cells and *p53*-null cells. **e–j**, Western blot analysis of SLC7A11 expression in Cal-33 (**e**, p53^R175H), TOV-112D (**f**, p53^R175H), HuCCT1 (**g**, p53^R175H), T-47D (**h**, p53^L194F), BT-549 (**i**, p53^R249S) and BT-474 (**j**, p53^E285K) cells treated with NC siRNA or p53 siRNA for 48 h. **k–m**, Western blot analysis of SLC7A11 expression in Cal-33 (**k**), HuCCT1 (**l**) and KLE (**m**) cells treated with NC siRNA, p53 siRNA, BACH1 siRNA or p53 siRNA + BACH1 siRNA for 48–72 h. Cal-33 cells, 72 h; HuCCT1 cells, 48 h; KLE cells, 56 h. **n**, Western blot analysis of SLC7A11 expression in Cal-33 Ctrl, *p53*^R175H−/−, *BACH1*^−/− and *p53*^R175H−/−*BACH1*^−/− cells. Two clones were analyzed for each type of CRISPR knockout cells. Data represent mean of three technical replicates. The experiments (**a**,**d–n**) were repeated twice with similar results and representative results are shown.

Cal-33 cells led to downregulation of SLC7A11 expression (Fig. 2e). Similar results were also obtained in other native p53[R175H] expressing cell lines including HuCCT1 and TOV-112D (Fig. 2f,g); however, knockdown of endogenous mutant p53 in native p53[L194F] expressing human breast cancer T-47D cell line had no obvious effect on SLC7A11 expression (Fig. 2h). The same conclusion was evident in the native p53[R249S], p53[E285K] or p53[R306-Stop] expressing human breast cancer cell lines BT-549, BT-474 and HCC1937, respectively (Fig. 2i,j and Extended Data Fig. 2c). These data suggest that p53[R175H] has a specific GOF by upregulating SLC7A11 expression.

Moreover, we examined whether the p53[R175H]-mediated effect on SLC7A11 expression is BACH1-dependent. As shown in Fig. 2k, knockdown of p53[R175H] downregulated SLC7A11 expression but knockdown of both p53[R175H] and BACH1 significantly abrogated the downregulation of SLC7A11 induced by loss of p53[R175H] expression. Similar results were also obtained in p53[R175H] expressing human liver bile duct carcinoma HuCCT1 cell line and human endometrial carcinoma KLE cell line (Fig. 2l,m). A similar conclusion was also made by monitoring the messenger RNA levels in those experiments (Extended Data Fig. 2d–f). Moreover, by using the CRISPR method, we also established Cal-33 derived p53[R175H–/–], BACH1^{–/–} and p53[R175H–/–]BACH1^{–/–} cell lines. As shown in Fig. 2n, the levels of SLC7A11 were indeed downregulated in the p53[R175H–/–] cells but the downregulation of SLC7A11 was completely abolished in the p53[R175H–/–]BACH1^{–/–} cells. Moreover, we expanded the similar analysis to other BACH1 targets involved in iron metabolism and oxidative stress responses, including glutamate-cysteine ligase modifier subunit (GCLM), heme oxygenase-1 (HMOX1), ferritin heavy chain 1 (FTH1) and ferritin light chain 1 (FTL). As expected, BACH1 is able to regulate the expression of all these targets (Extended Data Fig. 2g–j); nevertheless, SLC7A11 is the only target that can be significantly modulated by p53[R175H] expression. These results demonstrate that p53[R175H] has a unique GOF property by abrogating BACH1-mediated transcriptional repression of SLC7A11.

As the SLC7A11 levels are critical for modulating ferroptotic responses in human cancers[35,37], it is very likely that p53[R175H]-mediated regulation on SLC7A11 expression through BACH1 has a direct impact on ferroptotic responses in cancer cells. To that end, we first performed ferroptosis assays in the established Cal-33 derived p53[R175H–/–], BACH1^{–/–} and p53[R175H–/–]BACH1^{–/–} cell lines. Indeed, p53[R175H] loss significantly sensitized Cal-33 cells to reactive oxygen species (ROS)-mediated ferroptosis in p53[R175H–/–] cells upon the treatment of tert-butyl hydroperoxide (TBH) (for generating ROS) but cell death was completely rescued in p53[R175H–/–]BACH1^{–/–} cells or by ferrostatin-1 (Ferr-1), a well-known ferroptosis inhibitor (Fig. 3a–c). Similar results were also obtained when specific short-interfering (si)RNAs were used for knockdown of p53[R175H] or BACH1 in Cal-33 cells (Extended Data Fig. 2k). Consistently, the lipid peroxidation level was significantly higher in p53[R175H–/–] cells compared to Ctrl, BACH1^{–/–} and p53[R175H–/–]BACH1^{–/–} cells upon ROS stress

(Fig. 3d,e). We also examined the effects of these cells upon the treatment of erastin[38]. Again, although very low levels of ferroptosis were observed in the control Cal-33 cells, high levels of ferroptosis were observed in p53[R175H–/–] cells but were diminished in p53[R175H–/–]BACH1^{–/–} cells under the same conditions, or by treatment with Ferr-1 (Fig. 3f). Similar results were also obtained in mouse p53[R172H/R172H] sarcoma cells (Extended Data Fig. 2l,m). As shown in Extended Data Fig. 2l,m, consistent with the above data, erastin-induced ferroptosis was sensitized in p53[R172H–/–] cells but not in BACH1^{–/–} cells. Taken together, these data established that BACH1-dependent ferroptosis is suppressed by p53[R175H] (or mouse p53[R172H]).

We next examined whether BACH1-mediated tumor growth suppression is also abrogated by p53[R175H] in xenograft tumor models. To that end, Cal-33-derived p53[R175H–/–], BACH1^{–/–} and p53[R175H–/–]BACH1^{–/–} cells were mixed with Matrigel and injected subcutaneously into nude mice to establish xenograft tumors. Notably, although loss of BACH1 alone had no obvious effect on the growth of Cal-33 tumor xenografts (BACH1^{–/–} versus Ctrl; Fig. 3g,h), the growth of p53[R175H–/–] Cal-33 xenografts was significantly accelerated upon loss of BACH1 expression (p53[R175H–/–]BACH1^{–/–} versus p53[R175H–/–], Fig. 3g,h). These data indicate that BACH1 is able to suppress tumor growth but this activity is abrogated in the presence of p53[R175H] expression (Extended Data Fig. 9 and Discussion provide additional evidence). As upregulation of PTGS2 has been reported as a marker of ferroptosis[39], we examined PTGS2 levels in the xenograft tumors. Indeed, upregulation of PTGS2 observed in p53[R175H–/–] tumors was abolished upon loss of BACH1 in p53[R175H–/–]BACH1^{–/–} tumors, whereas no obvious effect was detected in p53[R175H]-expressing cells (BACH1^{–/–} versus Ctrl) (Fig. 3i). Moreover, high lipid peroxidation levels were detected in the tumors derived from p53[R175H–/–] cells but the increasing levels were again abrogated in the absence of BACH1 expression (Fig. 3j,k). Furthermore, we performed a number of additional assays to support the importance of SLC7A11 regulation induced by p53[R175H] including the immunohistochemistry (IHC) staining of TUNEL (apoptosis marker), 4-HNE (ferroptosis marker), SLC7A11 and Ki67 (cell proliferation marker) using paraffin sections of the xenograft tumors (Extended Data Fig. 3a–i). These data indicate that BACH1-mediated tumor growth suppression is abrogated in the presence of p53[R175H] expression through modulating ferroptotic cell death.

Finally, to examine whether p53[R175H]-mediated regulation of SLC7A11 directly contributes to regulating tumor growth, we established Cal-33 SLC7A11^{–/–} cells by the CRISPR method to examine the effect of SLC7A11 in tumor growth (Extended Data Fig. 4a). As shown in Extended Data Fig. 4b–e, loss of SLC7A11 expression significantly suppressed tumor growth in a xenograft tumor model with increased levels of 4-HNE, a marker for ferroptosis. Moreover, as the levels of SLC7A11 were dramatically reduced in p53[R175H–/–] cells, we also ectopically overexpressed SLC7A11 in those Cal-33 p53[R175H/-] cells to test whether overexpression of SLC7A11 is able to rescue the effect by loss

**Fig. 3 | p53[R175H] effectively suppresses BACH1-mediated ferroptosis to promote primary tumor growth in xenograft tumor mouse model.**
**a**, Representative images of ferroptotic cell death in Cal-33 Ctrl, p53[R175H–/–], BACH1^{–/–} and p53[R175H–/–]BACH1^{–/–} cells treated with TBH. Scale bar, 50 μm. **b**, Zoomed-in image in dotted box in **a**. Red arrows indicate cells undergoing ferroptotic cell death. **c**, Cell death assay for Cal-33 Ctrl, p53[R175H–/–], BACH1^{–/–} and p53[R175H–/–]BACH1^{–/–} cells treated with 1 mM TBH for 10 h in presence or absence of 5 μM Ferr-1 (n = 3 technical cell culture replicates). The experiment was repeated three times with similar results. **d**, C11-BODIPY staining and subsequent FACS analysis of lipid peroxidation of Cal-33 Ctrl, p53[R175H–/–], BACH1^{–/–} and p53[R175H–/–]BACH1^{–/–} cells treated with 0.85 mM TBH for 1 h. **e**, Quantitative analysis of lipid peroxidation level, related to **d**. Lipid peroxidation was expressed as the ratio of oxidized probe signal (excitation/emission 488/530 nm) over non-oxidized probe signal (excitation/emission 561/585 nm) with n = 3 technical cell culture replicates. The experiment was repeated twice with similar results. **f**, Cell death assay for Cal-33 Ctrl, p53[R175H–/–], BACH1^{–/–} and p53[R175H–/–]BACH1^{–/–} cells
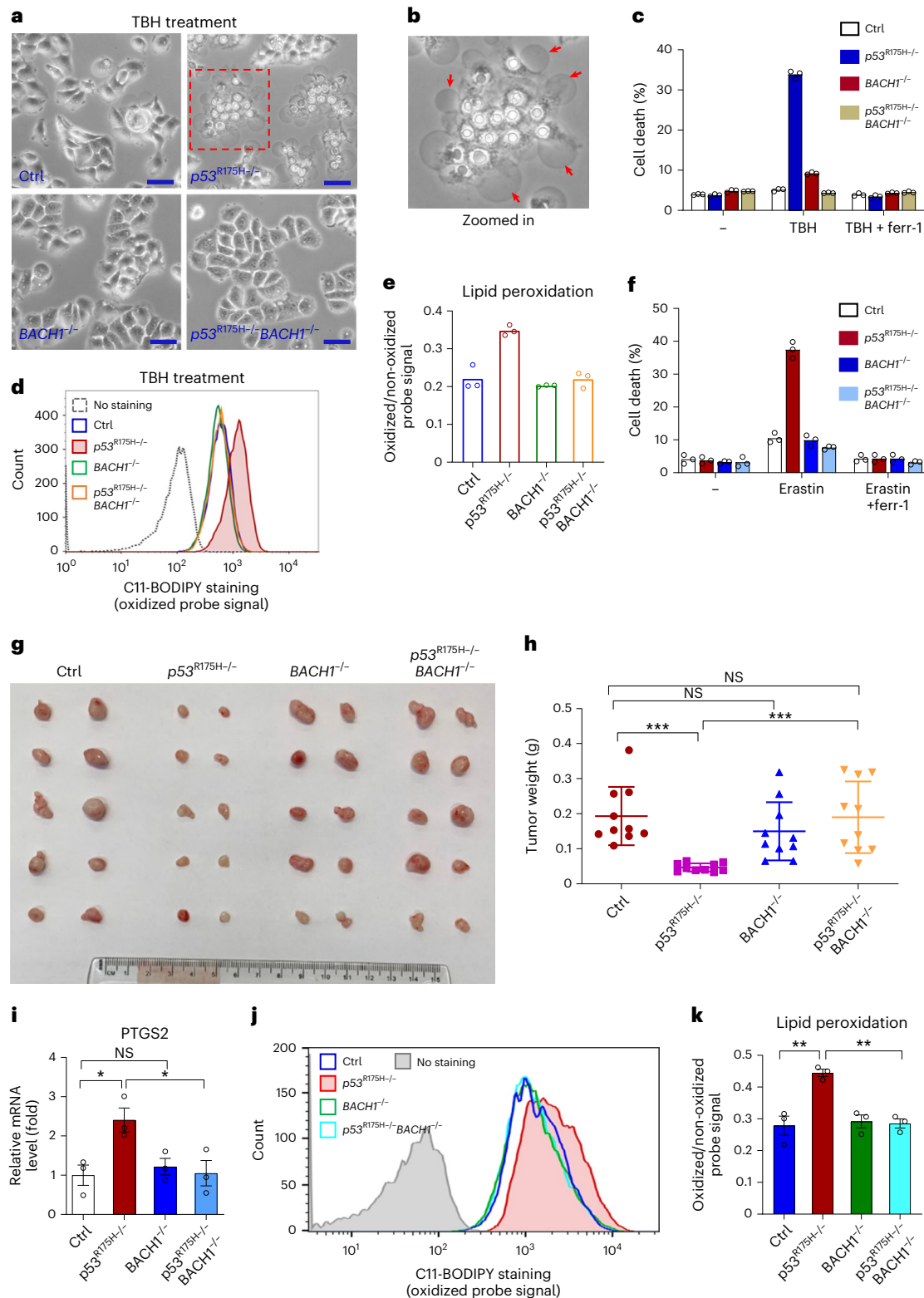
treated with 10 μM erastin for 72 h in the presence or absence of 5 μM Ferr-1 with n = 3 technical cell culture replicates. The experiment was repeated three times with similar results. **g**, Tumors isolated from nude mice implanted with Cal-33 Ctrl, p53[R175H–/–], BACH1^{–/–} and p53[R175H–/–]BACH1^{–/–} cells. Mice were killed at day 19 (n = 10 tumors). **h**, Tumor weights (n = 10 tumors). P values (from left to right), <0.0001; 0.2569; 0.9302; and 0.0004. **i**, qPCR analysis of PTGS2 mRNA level in Ctrl, p53[R175H–/–], BACH1^{–/–} and p53[R175H–/–]BACH1^{–/–} tumors (n = 3 tumors). P values (from left to right), 0.0242; 0.5517; and 0.0378; **j**, C11-BODIPY staining and subsequent FACS analysis of lipid peroxidation in cells digested from Cal-33 Ctrl, p53[R175H–/–], BACH1^{–/–} and p53[R175H–/–]BACH1^{–/–} tumors. **k**, Quantitative analysis of lipid peroxidation level, related to **j**. Lipid peroxidation was expressed as the ratio of oxidized probe signal (excitation/emission 488/530 nm) over non-oxidized probe signal (excitation/emission 561/585 nm) in n = 3 tumors. P values (from left to right), 0.0068 and 0.001. Two-tailed Student's t-test was used for statistical analysis. NS, not significant, *P < 0.05, **P < 0.01, ***P < 0.001; Data (**c**,**e**,**f**) represent mean of three technical replicates. Data (**h**,**i**,**k**) represent mean + s.e.m.
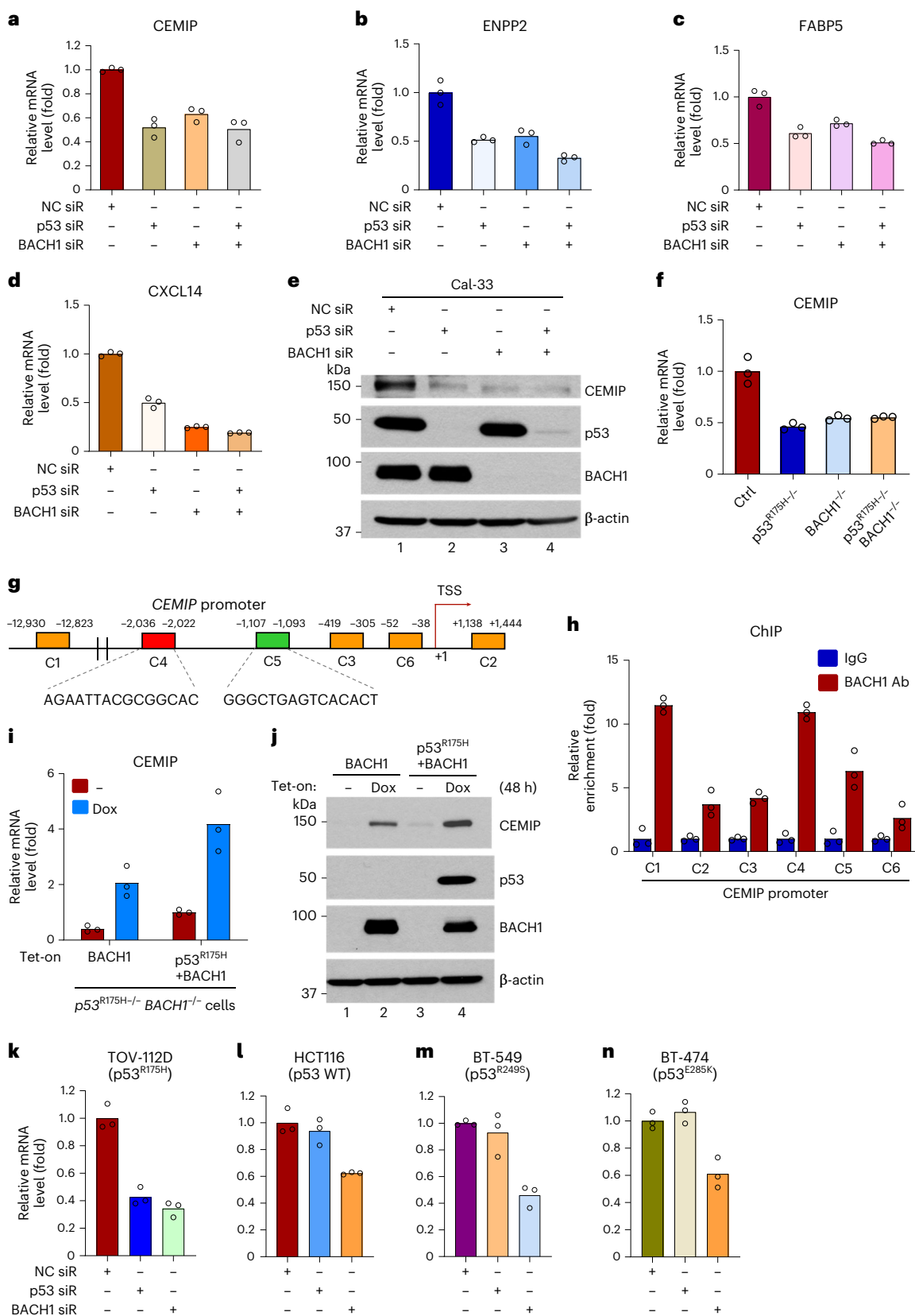
of p53[R175H] in tumor growth. Indeed, overexpression of SLC7A11 ectopically in *p53*[R175H−/−] cells was able to promote tumor growth (Extended Data Fig. 4f–h). Consistently, the 4-HNE levels were also reduced upon SLC7A11 expression in those tumors (Extended Data Fig. 4i,j), suggesting that the ferroptosis response is suppressed by SLC7A11 expression. As expected, loss of SLC7A11 expression dramatically sensitized the cells to the ferroptosis responses induced by either erastin or TBH; conversely, overexpression of SLC7A11 in *p53*[R175H−/−] cells protected the

cancer cells from erastin- or TBH-induced ferroptosis (Extended Data Fig. 4k–m). These data demonstrate that p53[R175H] acts as a repressor for ferroptosis by abrogating BACH1-mediated downregulation of SLC7A11 to promote tumor growth.

## p53[R175H] enhances the pro-metastatic activity of BACH1
As both BACH1 and p53[R175H] are able to promote metastasis, we examined whether the p53[R175H] is also involved in regulating BACH1-mediated



**a** TBH treatment — Ctrl, *p53*[R175H−/−], *BACH1*^{−/−}, *p53*[R175H−/−]*BACH1*^{−/−}

**b** Zoomed in

**c** Cell death (%) — Ctrl, *p53*[R175H−/−], *BACH1*^{−/−}, *p53*[R175H−/−]*BACH1*^{−/−}; conditions −, TBH, TBH + ferr-1

**d** TBH treatment — C11-BODIPY staining (oxidized probe signal); No staining, Ctrl, *p53*[R175H−/−], *BACH1*^{−/−}, *p53*[R175H−/−] *BACH1*^{−/−}

**e** Lipid peroxidation — Oxidized/non-oxidized probe signal; Ctrl, *p53*[R175H−/−], BACH1^{−/−}, *p53*[R175H−/−] BACH1^{−/−}

**f** Cell death (%) — Ctrl, *p53*[R175H−/−], *BACH1*^{−/−}, *p53*[R175H−/−] *BACH1*^{−/−}; conditions −, Erastin, Erastin +ferr-1

**g** Ctrl, *p53*[R175H−/−], *BACH1*^{−/−}, *p53*[R175H−/−]*BACH1*^{−/−}

**h** Tumor weight (g) — Ctrl, *p53*[R175H−/−], *BACH1*^{−/−}, *p53*[R175H−/−]*BACH1*^{−/−}; NS, NS, ***, ***

**i** PTGS2 — Relative mRNA level (fold); Ctrl, p53[R175H−/−], BACH1^{−/−}, p53[R175H−/−] BACH1^{−/−}; *, NS, *

**j** C11-BODIPY staining (oxidized probe signal); Ctrl, *p53*[R175H−/−], *BACH1*^{−/−}, *p53*[R175H−/−]*BACH1*^{−/−}, No staining

**k** Lipid peroxidation — Oxidized/non-oxidized probe signal; Ctrl, p53[R175H−/−], BACH1^{−/−}, p53[R175H−/−] BACH1^{−/−}; **, **

metastasis activity. Although BACH1 acts primarily as a transcriptional repressor for antioxidant genes, including *SLC7A11* (refs. [26,40]), recent studies indicate that BACH1 promotes metastasis through activating pro-metastatic gene expression[29]. Upon analysis of RNA-seq data (Supplementary Table 1), we found that a number of potential metastasis genes were downregulated upon knockdown of p53[R175H] or BACH1,

including cell migration-inducing hyaluronidase 1 (*CEMIP*), *CXCL14*, fatty acid-binding protein 5 (*FABP5*) and autotaxin (*ENPP2*)[41–44] (Fig. 4a–d). Among these targets, we found that CEMIP, also called KIAA1199 or HYBID, is particularly noteworthy as it acts as a critical metastatic driver gene in multiple cancer types[41,45]. CEMIP was detected in exosomes produced by metastatic tissues from patients with breast and lung

**Fig. 4 | *CEMIP*, a pro-metastatic gene, is a direct target of BACH1 and BACH1-mediated induction of CEMIP is upregulated by p53^R175H expression.** **a–d**, qPCR validation of p53^R175H and BACH1 co-upregulated pro-metastatic genes in Cal-33 cells treated with NC siRNA, p53 siRNA, BACH1 siRNA or p53 siRNA + BACH1 siRNA (twice siRNA transfections at day 1 and day 3). CEMIP (**a**); ENPP2 (**b**); FABP5 (**c**); and CXCL14 (**d**). $n = 3$ technical replicates. The experiment was repeated three times with similar results. **e**, Western blot analysis of CEMIP protein level in Cal-33 cells treated with NC siRNA, p53 siRNA, BACH1 siRNA or p53 siRNA + BACH1 siRNA. **f**, qPCR analysis of CEMIP mRNA expression in Cal-33 Ctrl, *p53^R175H−/−*, *BACH1^−/−* and *p53^R175H−/−BACH1^−/−* cells ($n = 3$ technical replicates). The experiment was repeated twice with similar results. **g**, Mapping of CEMIP promoter region. TSS, transcription start site. **h**, ChIP analysis of the recruitment of BACH1 to different regions of CEMIP promoter. C1, C2, C3, C4, C5 and C6 are six potential sites that match the consensus BACH1-binding sequence. **i**, qPCR analysis of CEMIP mRNA expression in BACH1 inducible cells and p53^R175H/BACH1 double-inducible cells treated with or without 2 μg ml^−1 doxycycline for 48 h. $n = 3$ technical replicates (**h,i**). The experiments were repeated twice with similar results. **j**, Western blot analysis of CEMIP expression in BACH1-inducible cell and p53^R175H/BACH1 double-inducible cell treated with or without 2 μg ml^−1 doxycycline for 48 h. **k–n**, qPCR analysis of CEMIP expression in TOV-112D (**k**, p53^R175H), HCT116 (**l**, p53 WT), BT-549 (**m**, p53^R249S) and BT-474 (**n**, p53^E285K) cells treated with NC siRNA or p53 siRNA or BACH1 siRNA for 48 h ($n = 3$ technical replicates). The experiment was repeated twice with similar results. Data represent mean of three technical replicates.

cancer. Moreover, high CEMIP expression levels are significantly associated with accelerated metastasis progression and poorer survival[41].

To dissect the role of both BACH1 and p53^R175H in regulating CEMIP expression, we first examined whether CEMIP is a transcriptional activation target of BACH1 and whether p53^R175H-mediated regulation of CEMIP expression is dependent upon BACH1. As shown in Fig. 4e, endogenous CEMIP was reduced upon siRNA-mediated knockdown of p53^R175H, whereas siRNA-mediated knockdown of BACH1 alone or both BACH1 and p53^R175H produced the same effects. Similar results were also obtained in CRISPR-mediated knockout Cal-33 cell lines: *p53^R175H−/−*, *BACH1^−/−* and *p53^R175H−/−BACH1^−/−* (Fig. 4f). Moreover, human *CEMIP* gene promoter region has six potential sites (C1, C2, C3, C4, C5 and C6) that contain the consensus binding element for BACH1 (Fig. 4g). Indeed, chromatin immunoprecipitation (ChIP) showed significant recruitment of BACH1 to C1, C4 and C5, but at lower levels to other sites (Fig. 4h), suggesting that CEMIP is indeed a direct target of BACH1. Next, we examined whether p53^R175H promotes BACH1-induced CEMIP expression. To this end, we first made BACH1 Tet-on inducible cells and p53^R175H/BACH1 Tet-on inducible cells. As shown in Fig. 4i,j, both mRNA levels and protein levels of CEMIP were upregulated upon BACH1 induction; more notably, BACH1-induced CEMIP expression was further enhanced in the presence of p53^R175H expression (Fig. 4i,j). These data demonstrate that CEMIP is a direct target of BACH1 and that BACH1-mediated induction of CEMIP is enhanced by p53^R175H expression.

To validate the specific regulation on CEMIP expression by p53^R175H, we conducted an RNAi experiment in a number of cell lines. As expected, knockdown of p53 or BACH1 in the p53^R175H native cell line TOV-112D dramatically downregulated CEMIP mRNA levels (Fig. 4k). In contrast, knockdown of p53 in wild-type p53-expressing HCT116 cells or in other p53 mutant native cell lines BT-549 (p53^R249S) and BT-474 (p53^E285K) showed no significant effect on expressing levels of CEMIP mRNA (Fig. 4l–n).

Next, we examined whether activation of CEMIP by BACH1 and p53^R175H is critically involved in regulating tumor metastasis activity. To this end, we first tested the role of p53^R175H and BACH1 in metastasis by using the well-established tail vein injection approach (Extended Data Fig. 5a)[14,46]. As shown in Fig. 5a, high levels of lung metastases lesions were indeed detected in mice 6 weeks after tail vein injection of native Cal-33 cells but no obvious metastatic lesions were detected in either livers or kidneys (Fig. 5b and Extended Data Fig. 5b,d,e). Notably, the number of metastatic lesions and the total metastatic area were dramatically reduced upon loss of either p53^R175H or BACH1 or both (Fig. 5a,c and Extended Data Fig. 5c), suggesting that both p53^R175H and BACH1 are critical for lung metastasis. As both CEMIP levels and metastasis activity were dramatically reduced in the tumors derived from *p53^R175H−/−* cells, we tested whether ectopic expression of CEMIP is able to rescue the defects of the metastatic potential in these cells (Fig. 5d). As shown in Fig. 5e, ectopic expression of CEMIP in *p53^R175H−/−* Cal-33 cells largely restored the metastatic potential of these cells (Fig. 5e–g). Moreover, we established the Cal-33 CEMIP knockout cell lines by the CRISPR technology (Extended Data Fig. 5f) and then tested these cells in the tail vein injection metastasis tumor model. As shown in Extended Data Fig. 5g–i, loss of CEMIP expression remarkably reduced the levels of lung metastasis. These data demonstrate that p53^R175H accelerates tumor metastasis by upregulating CEMIP, a pro-metastatic target of BACH1.

Nevertheless, it remains possible that the p53^R175H-mediated effect on SLC7A11 expression and ferroptosis also contributes to tumor metastasis. To this end, we established both *SLC7A11*-null Cal-33 cells and the *p53^R175H−/−* Cal-33 cells ectopically overexpressed SLC7A11 to examine the effects in the tumor metastasis model. As showed in Extended Data Fig. 6a–c, neither loss of SLC7A11 in Cal-33 cells nor SLC7A11 overexpression in *p53^R175H−/−* Cal-33 cells was able to significantly affect the levels of tumor metastasis. Consistent with the above results, loss of ACSL4 expression, a well-known key mediator of ferroptosis failed to affect the levels of the lung metastasis of Cal-33 cells (Extended Data Fig. 6d–f). Together, these data indicate that p53^R175H-mediated regulation on tumor growth and metastasis acts through different cellular targets (SLC7A11 versus CEMIP).

To corroborate our findings, we used *p53^R172H/R172H* mouse sarcoma cells to examine whether p53^R172H-BACH1 interaction is critical for tumor metastasis. To this end, we isolated *p53^R172H/R172H* cells from spontaneously-developed sarcoma tumors derived from *p53^R172H/R172H*

**Fig. 5 | BACH1/p53^R175H-mediated regulation of CEMIP expression is critical for lung metastasis. a**, Representative fluorescence images of lungs infiltrated with Cal-33 Ctrl, *p53^R175H−/−*, *BACH1^−/−* and *p53^R175H−/−BACH1^−/−* tumors. Each red spot represents a metastatic node. Scale bar, 500 μm. Images are from four representative lungs from seven mice (each group) with similar results. **b**, Zoomed-in image in dotted box in **a**. White arrows indicate the metastatic nodes in lung tissues. **c**, Quantitative analysis of number of metastases in lungs using BZ-X-800 Analyzer software, related to **a** ($n = 7$ mice for each group). $P$ values (from left to right), <0.0001; <0.0001; <0.0001; 0.7421; and 0.2123. **d**, Western blot analysis of CEMIP, p53 and BACH1 expression in Cal-33 Ctrl cells, *p53^R175H−/−* cells and *p53^R175H−/−* cells overexpressing CEMIP, related to **e**. Experiment was repeated three times with similar results and a representative result is shown. **e**, In vivo luminescence imaging of mice 4 weeks after tail vein injection of 0.5 million luciferase-carrying Cal-33 Ctrl cells, *p53^R175H−/−* cells, or *p53^R175H−/−* cells overexpressing CEMIP. Mice were intraperitoneally (i.p.) injected with luciferase substrate D-luciferin and imaged on an IVIS Spectrum Optical Imaging System ($n = 5$ mice for each group). **f,g**, Quantitative analysis of total counts of luminescence (**f**) and average counts of luminescence (**g**) in lungs, related to **e** ($n = 5$ mice for each group). $P$ values in **f** (from left to right), 0.0012 and 0.0235. $P$ values in **g** (from left to right), 0.0005 and 0.0096. **h**, Diagram of differential regulation of BACH1-mediated tumor metastasis versus ferroptosis by p53^R175H. On the one side, p53^R175H suppresses BACH1-mediated ferroptosis through its transcriptional targets such as SLC7A11 to promote tumor growth; on the other side, p53^R175H accelerates the tumor metastasis activity by upregulating the pro-metastatic targets of BACH1 such as CEMIP. Two-tailed Student's $t$-test was used for statistical analysis. NS, not significant, *$P < 0.05$, **$P < 0.01$, ***$P < 0.001$; Data represent mean + s.e.m.

mice and made isogenic *p53*^R172H−/− and *p53*^R172H/R172H*BACH1*^−/− sarcoma cells derived from these *p53*^R172H/R172H cells to examine the effects in tumor metastasis. Indeed, the number of metastatic lesions and the total metastatic area were dramatically reduced upon loss of either p53^R175H or BACH1 (Fig. 6a,c,d), suggesting that both p53^R175H and BACH1 are critical for the metastasis activity of these *p53*^R172H/R172H sarcoma cells. Moreover, although CEMIP was highly expressed in these parental *p53*^R172H/R172H sarcoma cells, upon loss of the expression of either p53^R172H or BACH1, the expression levels of CEMIP were dramatically downregulated in *p53*^R172H−/− or *BACH1*^−/− sarcoma cells (Fig. 6b).

Furthermore, we examined whether ectopic p53^R175H expression promotes tumor metastasis and whether this activity is BACH1-dependent in human colorectal cancer HCT116 *p53*-null cells. Thus, we first established Tet-on p53^R175H inducible cell line derived from the HCT116 *p53*^−/− cells and a Tet-on p53^R175H inducible cell line in the *BACH1/p53* double-null background by the CRISPR technology (Fig. 6e). As expected, very low levels of lung metastatic lesions were detected in the mice 8 weeks after tail vein injection of these parental HCT116 *p53*^−/− cells (Fig. 6f,g). Notably, upon ectopic expression of p53^R175H, the total metastatic area was dramatically increased; however, loss of BACH1
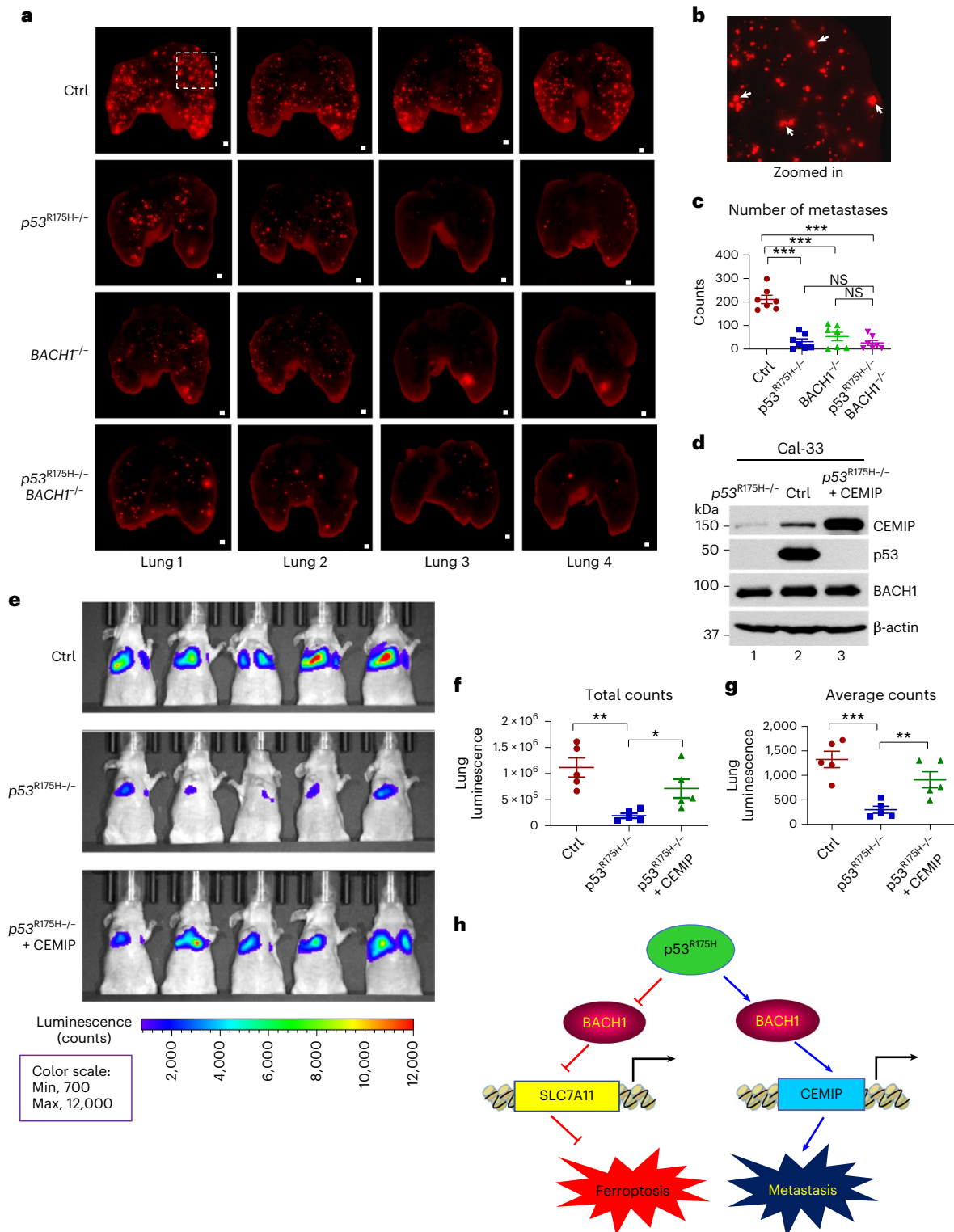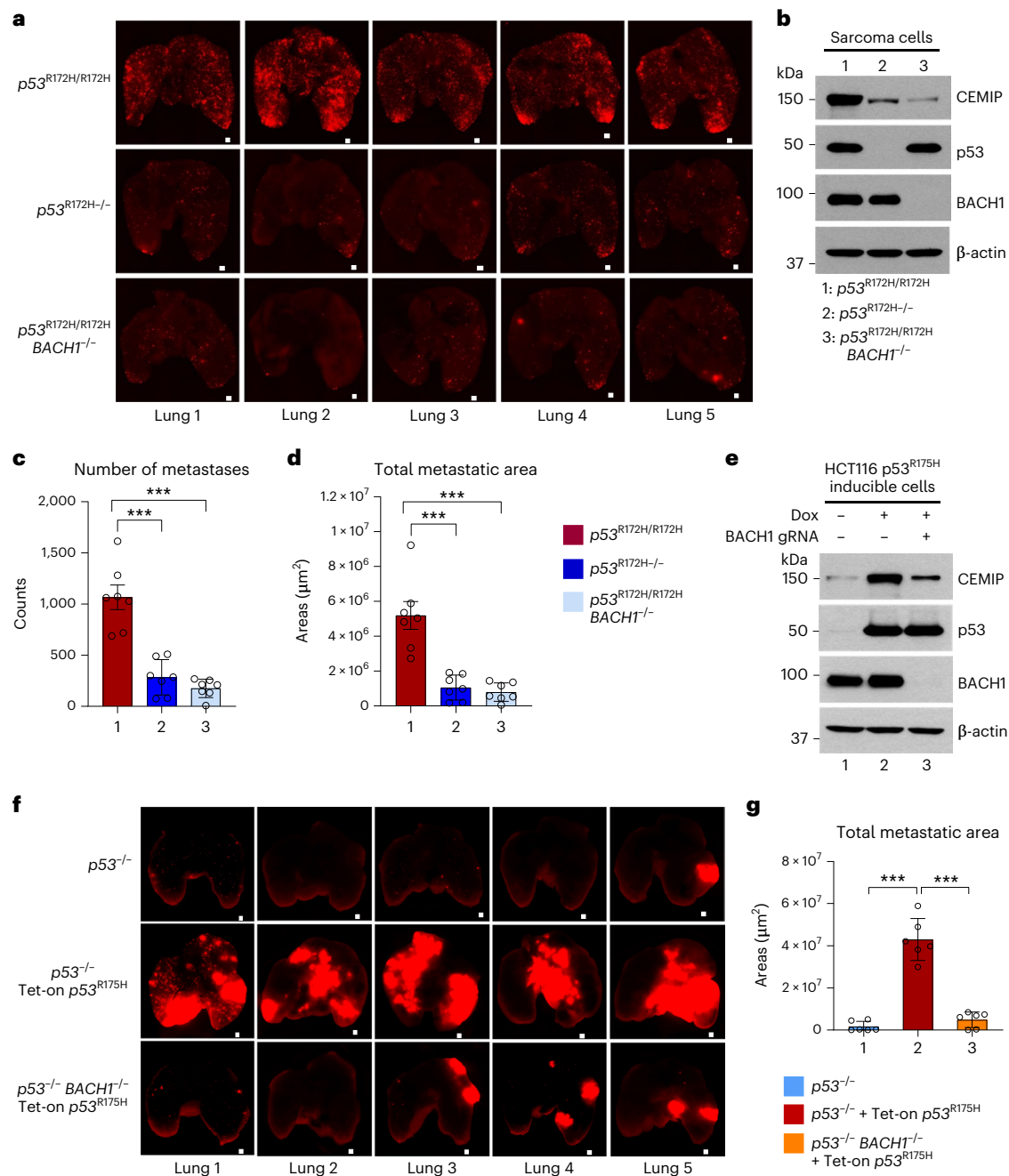
**Fig. 6 | BACH1/p53^R175H-mediated tumor metastasis in mouse sarcoma cell model and human HCT116 cell model. a–d,** Mouse sarcoma cells tail vein injection lung metastasis model. $p53^{R172H/R172H}$ sarcoma cells were derived from $p53^{R172H/R172H}$ transgenic mice and then transfected with Tomato fluorescence gene by lentivirus system. $p53^{R172H-/-}$ and $p53^{R172H/R172H}BACH1^{-/-}$ cells were made by CRISPR method from these $p53^{R172H/R172H}$ sarcoma cells. Representative images of sarcoma cells lung metastasis (**a**). Each red dot indicates a metastatic node. Scale bar, 500 μm. Images are five representative lungs from seven mice (each group) with similar results. Western blot analysis of CEMIP, p53 and BACH1 expression in sarcoma CRISPR knockout cells (**b**). Experiment was repeated three times with similar results and a representative result is shown. Quantitative analysis of number of metastases and total metastatic area (**c,d**). $n = 7$ mice for each group. $P$ values in **c** (from left to right), 0.0001 and <0.0001. $P$ values in **d** (from left to right), 0.0003 and 0.0002. **e–g,** HCT116 p53^R175H inducible cells tail vein injection lung metastasis model. HCT116 p53^R175H inducible cells were

made from HCT116 $p53^{-/-}$ cells by transfecting p53^R175H inducible plasmid. BACH1 gRNA was transfected into the p53^R175H inducible cells to make the $BACH1/p53^{R175H}$ double-null $p53^{R175H}$ inducible cells. p53^R175H inducible cells were pre-incubated with/without doxycycline for 48 h in vitro and injected into nude mice via tail vein injection (4 million per mouse) and maintained p53^R175H expression by feeding mice with a doxycycline (Dox) diet. **e,** Western blot analysis of CEMIP, p53 and BACH1 expression in HCT116 p53^R175H inducible cells in the presence or absence of doxycycline treatment and BACH1 guide RNA (gRNA) transfection. Experiment was repeated three times with similar results and a representative result is shown. **f,** Representative images of HCT116 cells lung metastasis. Red parts indicate the metastatic regions in lungs. Scale bar, 500 μm. Images are five representative lungs from six mice (each group) with similar results. **g,** Quantitative analysis of total metastatic area ($n = 6$ mice for each group). $P$ values (from left to right), <0.0001 and <0.0001. Two-tailed Student's $t$-test was used for statistical analysis. ***$P < 0.001$. Data represent mean + s.e.m.

expression completely abrogated the tumor metastasis effect induced by p53^R175H expression in those HCT116 $BACH1^{-/-}p53^{-/-}$ double-null cells (Fig. 6f,g). Again, we tested the levels of CEMIP in those tumor cells.

Indeed, although low levels of CEMIP were detected in these parental HCT116 $p53^{-/-}$ cells, upon ectopic expression of p53^R175H, CEMIP was dramatically induced; however, upregulation of CEMIP induced by p53^R175H

expression was largely abrogated upon loss of BACH1 expression (Fig. 6e). Together, these data confirm the role of the p53[R175H]-BACH1 interaction in regulating tumor metastasis in different cell types.

Finally, we also examined whether the p53[R175H]-BACH1 interaction is important in regulating tumor metastasis by using p53[R172H] knock in mice. Previous studies showed that loss of BACH1 alone (BACH1^{−/−}) had no obvious effect in normal development and tumorigenesis, whereas BACH1^{−/−}p53^{−/−} double-null mice succumbed to spontaneous cancers as frequently as p53-deficient mice[47]. Notably, Lang et al.[19] indicated that p53[R172H/+] mice were able to develop both primary tumors and metastatic tumors whereas p53[R172H/R172H] mice were tumor prone but died very early without obvious metastatic tumors. Thus, we crossed p53[R172H/+] mice with BACH1^{−/−} mice and obtained p53[R172H/+]BACH1^{−/−} mice and monitored the metastatic potential of these mice. As expected, metastatic tumors were observed in a significant number of p53[R172H/+] mice with a total metastatic rate (36.4%); notably, a much lower metastatic rate (15.7%) was detected in p53[R172H/+]BACH1^{−/−} mice, indicating that loss of BACH1 significantly reduces the metastatic potential of p53[R172H/+] mice (Fig. 7a–f). Consistently, loss of BACH1 also prolonged the survival of p53[R172H/+] mice (P = 0.0184) and the median survival was extended from 449 d (p53[R172H/+] mice) to 520 d (p53[R172H/+]BACH1^{−/−} mice) (Fig. 7g). Taken together, these data further support the notion that the p53[R175H]–BACH1 interaction is critically involved in regulating tumor metastasis.

## Mechanistic insight into p53[R175H] mediated effects on BACH1 in transcription

The above data reveal differential regulation of BACH1-mediated tumor growth versus tumor metastasis by p53[R175H]. On the one hand, p53[R175H] is able to suppress BACH1-mediated ferroptosis by abrogating its transcriptional repression of SLC7A11 to promote tumor growth; on the other hand, p53[R175H] accelerates tumor metastasis by upregulating BACH1-induced CEMIP (Fig. 5h). To dissect the mechanism by which p53[R175H] modulates BACH1-mediated transcription, we examined whether the DNA-binding activity of BACH1 on the SLC7A11 promoter is inhibited by p53[R175H] as p53[R175H] and BACH1 have opposite effects on SLC7A11 expression. As shown in Fig. 8a, ChIP assays revealed that loss of p53[R175H] did not significantly affect the DNA-binding activity of BACH1 on the promoter of SLC7A11; however, upon being coexpressed with BACH1, p53[R175H] was recruited to the SLC7A11 promoter in Cal-33 cells (Fig. 8b). Similar results were also obtained in a different cell line by the same approach (Extended Data Fig. 7a).

To further elucidate the mechanism of p53[R175H]-mediated effect in transcription, we tested the possibility that p53[R175H] may recruit a specific cofactor to regulate BACH1-mediated transcriptional repression. Notably, mass spectrometry analysis revealed that several peptides matched with a protein called LSD2 (also called KDM1B) from the p53[R175H]-associated protein complexes purified from human cancer cells (Extended Data Fig. 7b,c). Like LSD1 (also called KDM1A)[48], LSD2 is a FAD-dependent lysine-specific demethylase and recent studies showed that LSD2-mediated histone H3K4 demethylase activity is critical for transcriptional regulation[49–51].

Next, we examined the interactions between p53[R175H] and LSD2 in human cancer cells. Western blot analysis revealed that LSD2 was readily detected in the immunoprecipitated complexes of SFB-p53[R175H] but barely detectable in the immunoprecipitated complexes of SFB-p53 wild-type protein (Fig. 8c), suggesting that LSD2, like BACH1, preferentially interacts with the p53[R175H] protein. Moreover, we performed the co-immunoprecipitation assay in the p53[R175H] native cell line HuCCT1 and showed that the endogenous LSD2 was co-precipitated with endogenous p53[R175H] by an anti-p53-specific monoclonal antibody (DO-1) but not by the IgG control (Fig. 8d). Of note, a relatively weak interaction was detected between LSD2 and BACH1 by co-immunoprecipitation assays, but this interaction was significantly enhanced in the presence of p53[R175H] expression (Fig. 8e). Indeed, ChIP analysis with a LSD2-specific antibody revealed that coexpression of BACH1 and p53[R175H] significantly
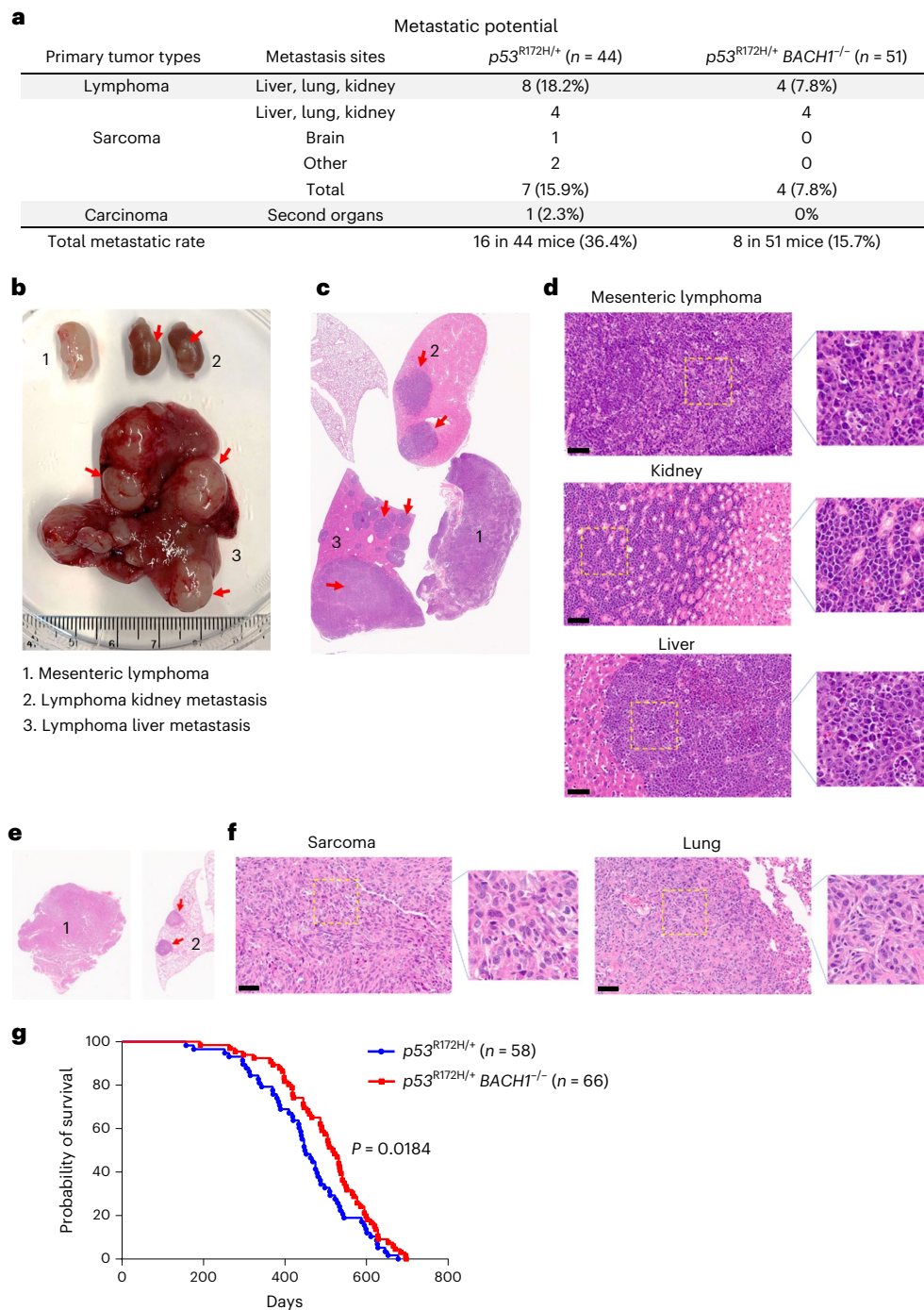
enhances the recruitment of LSD2 to the SLC7A11 promoter (Fig. 8f). Conversely, knockdown of either BACH1 or p53[R175H] attenuated the recruitment of LSD2 to the SLC7A11 promoter (Fig. 8g). Moreover, ChIP analysis with the LSD2 antibody revealed that overexpression of p53[R175H] in Cal-33 p53[R175H−/−]BACH1^{−/−} cells dramatically enhanced the enrichment of LSD2 to SLC7A11 promoter in the presence of wild-type BACH1 (Extended Data Fig. 7e). Notably, when the binding-defective BACH1 mutant (Δ466–515) was expressed in the cells (Extended Data Fig. 7d), the effects on the LSD2 recruitment induced by p53[R175H] were completely abrogated on SLC7A11 promoter (Extended Data Fig. 7e). These data demonstrate that the interaction between p53[R175H] and BACH1 is essential for LSD2-mediated regulation of SLC7A11.

LSD2 is a major histone H3K4 demethylase and several studies indicate that demethylase activity of LSD2 is critical for transcriptional activation[50,51]. As shown in Fig. 8h, although expression of LSD2 alone only slightly decreased the H3K4me2 methylation on the SLC7A11 promoter, coexpression of LSD2 with both BACH1 and p53[R175H] significantly enhanced the ability of LSD2 to reduce the levels of H3K4me2 methylation on the SLC7A11 promoter, suggesting that the p53[R175H]–LSD2 interaction is critical for modulating the transcription of SLC7A11 by recruiting the H3K4 demethylase. Moreover, siRNA-mediated knockdown of endogenous LSD2, similar to p53[R175H] knockdown, significantly reduced the levels of SLC7A11 expression in both p53[R175H]-expressing Cal-33 cells (Fig. 8i) and TOV-112D cells (Extended Data Fig. 7f). Indeed, the levels of SLC7A11 were also dramatically decreased in LSD2 knockout cells, suggesting that LSD2 is an essential cofactor of the SLC7A11 promoter (Fig. 8j). Taken together, these data demonstrate that p53[R175H] interacts with the coactivator LSD2 and that this interaction facilitates the recruitment of LSD2 to the target promoter of BACH1 for modulating the status of histone methylation, resulting in blocking of BACH1-mediated suppression of SLC7A11 transcription.

Notably, knockdown or knockout of LSD2 expression effectively abolished the expression of CEMIP, suggesting that LSD2 is also engaged in transcriptional activation of CEMIP (Fig. 8i,j). Next, we investigated whether the p53[R175H]–LSD2 interaction is involved in regulating BACH1-mediated activation of CEMIP. Consistent with above observations, ChIP assays revealed that loss of p53[R175H] expression did not influence the DNA-binding activity of BACH1 on the promoter of CEMIP (Fig. 8k) but p53[R175H] was also recruited to the promoter of CEMIP in the presence of BACH1 (Fig. 8l). Moreover, p53[R175H] expression promotes the recruitment of LSD2 to the promoter of CEMIP (Fig. 8m) but knockdown of either BACH1 or p53[R175H] attenuated the recruitment of LSD2 to the CEMIP promoter (Extended Data Fig. 7g). Consistently, when the p53[R175H] binding-defective BACH1 mutant (Δ466–515) was expressed in the cells, the effects on the LSD2 recruitment induced by p53[R175H] were abrogated on CEMIP promoter (Extended Data Fig. 7h). Moreover, the recruitment of LSD2 by p53[R175H] subsequently reduced the H3K4me2 methylation levels on the CEMIP promoter (Fig. 8n). These data indicate that p53[R175H] is able to enhance BACH1-mediated activation of CEMIP by promoting the recruitment of the coactivator LSD2 to the CEMIP promoter.

To further validate this notion, we conducted sequential ChIP assays[52] (first ChIP by BACH1 antibody, second by p53 DO-1 antibody and third by LSD2 antibody; Extended Data Fig. 8a) to study the recruitment of the protein complex p53[R175H]–BACH1–LSD2 to the BACH1 target promoters. We found that both LSD2 and p53[R175H] can be recruited by BACH1 to the promoters of SLC7A11 and CEMIP (Extended Data Fig. 8b,c). In contrast, both GCLM and FTH1 are transcriptional targets of BACH1, as the levels of both targets are upregulated upon BACH1 knockdown (Extended Data Fig. 2h,i); however, these two genes are not the targets of p53[R175H] as the sequential ChIP assay failed to detect any recruitment of this three-protein complex on the promoters of both GCLM and FTH1 (Extended Data Fig. 8d,e). These results support that the recruitment of this three-protein complex is critical for p53[R175H]-mediated regulation.

**a**

| Primary tumor types | Metastasis sites | Metastatic potential $p53^{R172H/+}$ ($n = 44$) | $p53^{R172H/+}$ $BACH1^{-/-}$ ($n = 51$) |
|---|---|---|---|
| Lymphoma | Liver, lung, kidney | 8 (18.2%) | 4 (7.8%) |
| Sarcoma | Liver, lung, kidney | 4 | 4 |
| | Brain | 1 | 0 |
| | Other | 2 | 0 |
| | Total | 7 (15.9%) | 4 (7.8%) |
| Carcinoma | Second organs | 1 (2.3%) | 0% |
| Total metastatic rate | | 16 in 44 mice (36.4%) | 8 in 51 mice (15.7%) |



b
1. Mesenteric lymphoma
2. Lymphoma kidney metastasis
3. Lymphoma liver metastasis

d
Mesenteric lymphoma
Kidney
Liver

f
Sarcoma
Lung

g

**Fig. 7 | BACH1 deficiency reduces the metastatic potential and prolongs the survival of $p53^{R172H/+}$ mice. a**, Metastatic rate of each type of tumors in $p53^{R172H/+}$ and $p53^{R172H/+}BACH1^{-/-}$ mice. $p53^{R172H/+}$ mice ($n = 44$); $p53^{R172H/+}BACH1^{-/-}$ mice ($n = 51$). **b**–**d**, Representative images of lymphoma liver and kidney metastasis in $p53^{R172H/+}$ mice. Images shown are representative of 16 mice with similar results. Gross image of mesenteric lymphoma and kidney and liver infiltrated with lymphoma (**b**). Low-power image of hematoxylin and eosin (H&E) staining of mesenteric lymphoma, liver and kidney (**c**). Red arrows indicate metastatic lesions. High-power (×40) images of H&E staining of mesenteric lymphoma and metastatic lesions in kidney and liver (**d**). Scale bar, 60 μm. **e**,**f**, Representative images of sarcoma lung metastasis in $p53^{R172H/+}BACH1^{-/-}$ mice. Images shown are representative of eight mice with similar results. Low-power image of H&E staining of primary sarcoma (1) and lung with metastatic nodes (2) (**e**). High-power (×40) image of H&E staining of primary sarcoma and metastatic nodes in lung (**f**). Scale bar, 60 μm. **g**, Survival curves of $p53^{R172H/+}$ and $p53^{R172H/+}BACH1^{-/-}$ mice. $p53^{R172H/+}$ mice ($n = 58$) and $p53^{R172H/+}BACH1^{-/-}$ mice ($n = 66$). $p53^{R172H/+}$ versus $p53^{R172H/+}BACH1^{-/-}$, $P = 0.0184$, calculated by log-rank (Mantel–Cox) test.

## Discussion

$p53^{R175H}$ is one of the major hotspot conformational mutants with purported GOF properties in tumorigenesis and metastasis. Nevertheless, the precise mechanism of $p53^{R175H}$-mediated action in these venues is not completely understood. Recent studies indicate that different mutant p53 display varied survival time, tumor spectrum and metastatic potential, raising the interesting possibility that the different GOFs induced by each individual p53 mutant may act through different mechanisms. By using a proteomic screen, we identified BACH1 as a major cellular factor that recognizes the DBD of p53 in a manner
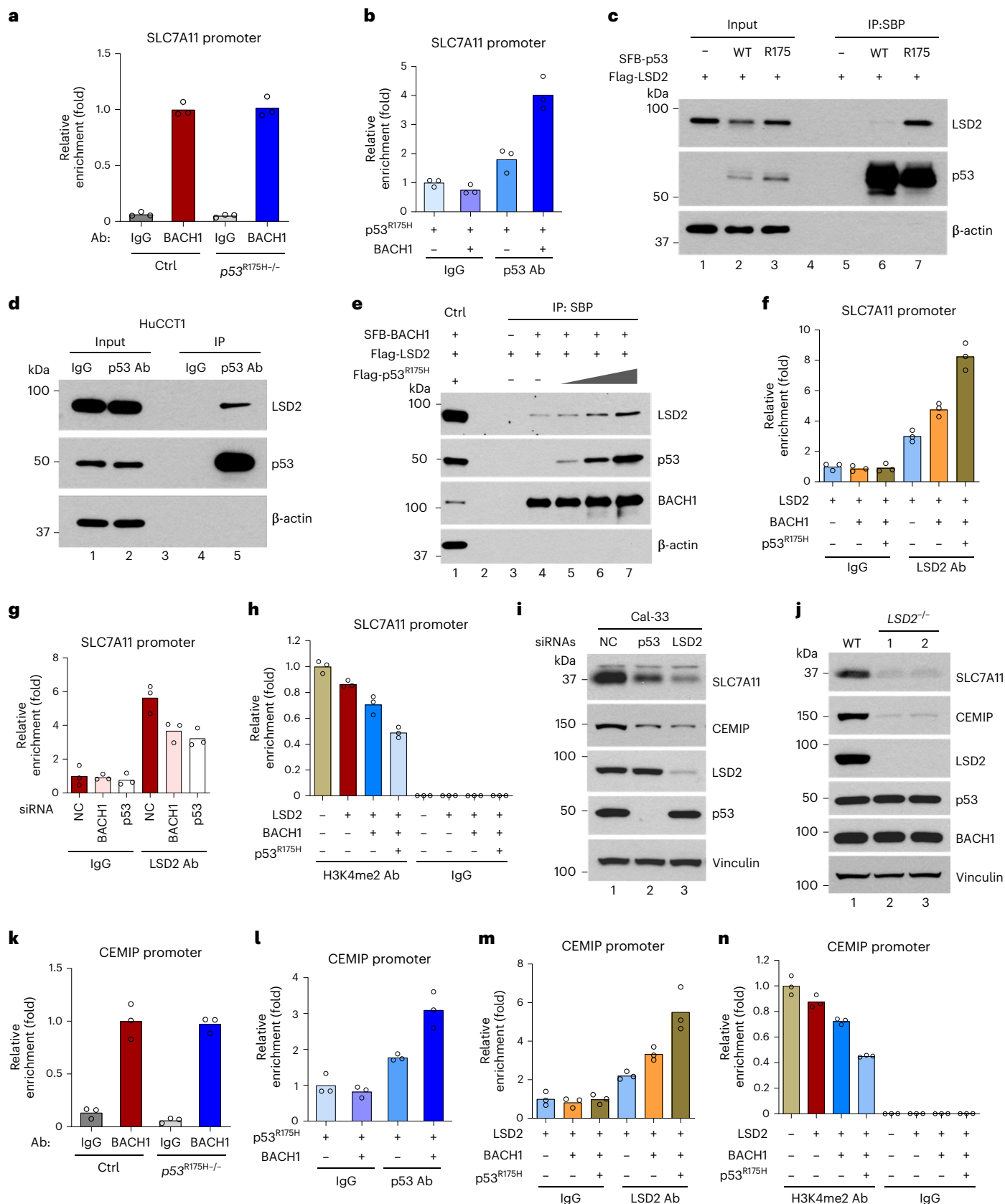
dependent upon its specific mutation. Of note, although BACH1 was reported to modestly affect wild-type p53 function in mouse cells[53], no obvious effect on p53-mediated tumor suppression was observed in BACH1-null mice[47], suggesting that the potential effects on wild-type p53 by BACH1 need further elucidation. BACH1 has opposite functions in transcription on two different types of target genes; on the one hand, it acts as a transcriptional repressor to downregulate a number of targets such as SLC7A11 critically involved in ferroptosis during oxidative stress responses; on the other hand, BACH1 can also function as a transcriptional activator to induce CEMIP to promote tumor metastasis.

**Fig. 8 | p53[R175H] differentially regulates the repression target versus the activation target of BACH1 through recruiting LSD2. a**, ChIP analysis of the recruitment of BACH1 to SLC7A11 promoter (−128 to −114) in Cal-33 Ctrl and *p53[R175H/-]* cells. **b**, ChIP analysis of the recruitment of p53[R175H] to SLC7A11 promoter in Cal-33 *p53[R175H−/−]BACH1^{−/−}* cells transfected with p53[R175H] plasmid alone or p53[R175H] + BACH1 plasmids. **c**, Co-IP of WT p53 or p53[R175H] with LSD2 in H1299 cells. Cells were co-transfected with SFB-WT p53/SFB-p53[R175H] and Flag-LSD2 and then IP was conducted with SBP. **d**, Endogenous co-IP of p53[R175H] and LSD2 and in HuCCT1 cells. Cell lysates were IPed with p53 DO-1 antibody. **e**, Co-IP of BACH1 and LSD2 in H1299 cells in presence of different amounts (0, 2, 5 or 10 μg) of p53[R175H]. **f**, ChIP analysis of the recruitment of LSD2 to SLC7A11 promoter in Cal-33 *p53[R175H−/−]BACH1^{−/−}* cells transfected with LSD2 alone, LSD2 + BACH1 or LSD2 + BACH1 + p53[R175H] plasmids. **g**, ChIP analysis of the recruitment of LSD2 to SLC7A11 promoter in Cal-33 cells treated with NC, BACH1 or p53 siRNA for 48 h. **h**, ChIP analysis of histone H3K4 dimethylation (H3K4me2) on SLC7A11 promoter

in Cal-33 *p53[R175H−/−]BACH1^{−/−}* cells transfected with control, LSD2, LSD2 + BACH1, or LSD2 + BACH1 + p53[R175H] plasmids. **i**, Western blot analysis of SLC7A11 and CEMIP expression in Cal-33 cells transfected with NC, p53 or LSD2 siRNA for 48 h. **j**, Western blot analysis of SLC7A11, CEMIP, p53 and BACH1 expression in WT and LSD2 CRISPR knockout clones (no. 1 and no. 2) of Cal-33 cells. **k**, ChIP analysis of the recruitment of BACH1 to CEMIP promoter (−2,036 to −2,022) in Cal-33 Ctrl and *p53[R175H−/−]* cells. **l**, ChIP analysis of the recruitment of p53[R175H] to CEMIP promoter in Cal-33 *p53[R175H−/−]BACH1^{−/−}* cells transfected with p53[R175H] plasmid alone or p53[R175H] + BACH1 plasmids. **m**, ChIP analysis of the recruitment of LSD2 to CEMIP promoter in Cal-33 *p53[R175H−/−]BACH1^{−/−}* cells transfected with indicated plasmids. **n**, ChIP analysis of histone H3K4 dimethylation on CEMIP promoter in Cal-33 *p53[R175H−/−]BACH1^{−/−}* cells transfected with indicated plasmids. *n* = 3 technical replicates (**a,b,f–h,k–n**). Experiments (**a–n**) were repeated twice with similar results. Data represent the mean of three technical replicates.

Our data demonstrate that p53[R175H] is able to suppress BACH1-mediated ferroptosis by abrogating its repression of SLC7A11 through the recruitment of LSD2 demethylase. This recruitment alters the status of histone methylation at the promoter of SLC7A11 and subsequently abrogating its transcriptional repression mediated by BACH1 (Extended Data Fig. 8f). Conversely, the recruitment of LSD2 demethylase by p53[R175H] to the promoter of CEMIP results in enhancing the transcriptional activation of CEMIP by BACH1 (Extended Data Fig. 8f).

Although loss of BACH1 alone had no significant effect on the tumor growth of the tumor xenografts expressing p53[R175H] (Fig. 3g), the growth of the *p53[R175H−/−]* Cal-33 xenografts was significantly accelerated upon loss of BACH1 expression (*p53[R175H−/−]BACH1^{−/−}* versus *p53[R175H−/−]*; Fig. 3g). These data indicate that BACH1 can suppress tumor growth in the *p53*-null background but this activity is abrogated in the presence of p53[R175H] expression, further supporting the important role of the BACH1–p53[R175H] interaction in modulating tumor growth. To provide the direct evidence that BACH1 is involved in suppression of tumor growth, we examined whether BACH1 expression is able to suppress tumor growth directly. To this end, we first established a Tet-on BACH1-inducible cell line derived from human colorectal cancer HCT116 *BACH1^{−/−}* cells (Extended Data Fig. 9a) and then tested whether re-induction of BACH1 expression in a *BACH1*-null background affects the tumor growth by using tumor xenograft model. As shown in Extended Data Fig. 9b–e, the growth of the xenograft tumors derived from those HCT116 cells was significantly reduced upon BACH1 expression. These data indicate that BACH1 expression is indeed able to suppress tumor growth.

Based upon our study, p53[R175H] is able to enhance the metastatic role of BACH1 by promoting its pro-metastatic targets expression but inhibit its tumor suppressive effects by abrogating the ability of BACH1 to activate ferroptosis. Thus, p53[R175H] is the perfect partner in crime for BACH1 in promoting both tumor growth and metastasis. To further evaluate the physiological relevance of this specific regulation by p53[R175H], we examined the expression levels of SLC7A11 and CEMIP among human patients carrying different p53 hotspot mutants by using the data from cBioPortal pan-cancer and specific cancers studies. As showed in Extended Data Fig. 10a,b, modest but significant correlations were observed between the levels of SLC7A11 and CEMIP in patients with p53[R175H] versus levels in patients with wild-type p53 or other hotspot mutants. Nevertheless, our findings seem at odds with a recent report[54], where Liu et al. claimed that p53 hotspot mutants, like wild-type p53, are able to induce SLC7A11 downregulation for potential tumor suppressive activity. As the functional studies by Liu et al. mainly focused on the effects on a small set of tumor cell lines in the presence of APR-246, a well-known p53-mutant targeting agent, future studies are required to investigate whether this discrepancy is caused by the APR-246 treatment.

Notably, the patients with cancer with higher expression of BACH1 have a shorter overall survival when those patients also have the *p53[R175H]*

mutation (*P* = 0.0233; Extended Data Fig. 10c); however, there are no statistical differences in survival between BACH1^{high} and BACH1^{low} patients with other hotspot *p53* mutations (*p53[R248Q/W]*, *p53[R273H]*, *p53[G245S]*, *p53[R249S]* and *p53[R248W]*) (Extended Data Fig. 10d–i). These data indicate that BACH1 expression is critical for the cancer patient survival with the *p53[R175H]* mutation. Furthermore, our study may also have significant implications in cancer therapy. For example, as the p53[R175H]–BACH1–LSD2 interaction is critical for both tumor growth and metastasis activities, targeting the BACH1–LSD2 axis may have specific effects to the treatment of human cancers with a specific *p53[R175H]* mutation. We found that inhibition of LSD2 expression effectively abolished the expression of both CEMIP and SLC7A11. Notably, LSD2 is overexpressed in multiple types of human cancers and that overexpression of LSD2 is also well correlated with aggressive tumor growth and poor prognosis[55–57]. Thus, LSD2 is a promising target to suppress both tumor metastasis and tumor growth in human cancers with the hotspot *p53[R175H]* mutation for a potential targeting therapy.

## Methods

The study research complies with all relevant ethical regulations. All experimental protocols were approved by the Institutional Animal Care and Use Committee of Columbia University.

### Cell line

KLE (CRL-1622), 293 T (CRL-3216), H1299 (CRL-5803), HCT116 (CCL-247), U2OS (HTB-96), TOV-112D, T-47D (HTB-133), BT-549 (HTB-122), BT-474 (HTB-20), MDA-MB-468 (HTB-132), MDA-MB-231 (HTB-26) and HCC1937 (CRL-2336) cells were purchased from the American Type Culture Collection. Cal-33 cells (cat. no. CSC-C0479) and HuCCT1 cells (cat. no. CSC-C9200W) were purchased from Creative Bioarray. *p53[R172H/R172H]* mice derived sarcoma cells were made in our laboratory. All cell lines were proven to be negative for *Mycoplasma* contamination. No cell lines used in this work were listed in the ICLAC database. All cells were cultured in a 37 °C incubator with 5% $CO_2$. All cancer cells, except for KLE, were cultured in high sugar DMEM supplemented with 10% FBS and 1% penicillin–streptomycin (Thermo Fisher Scientific, cat. no. 15140122). KLE cells were cultured in ATCC-formulated DMEM:F12 medium (cat. no. 30-2006) supplemented with 10% FBS and 1% penicillin–streptomycin.

### Mice

Balb/c NU/NU nude mice (CAnN.Cg-Foxn1nu/Crl, female, 6 weeks old) were purchased from Charles River Laboratories for xenograft and metastasis experiments. *p53[R172/+]* mice (male, 8 weeks old) were from K.P. Olive's laboratory and the genetic background was 129S$_4$/SvJae. We crossed *p53[R172H/+]* mice with wild-type C57BL/6J mice (female, 8 weeks old, purchased from the Jackson Laboratory) for at least eight generations to make them enriched for the C57BL/6J genetic background. *BACH1^{−/−}* mice were from K. Igarashi's laboratory and the genetic

background was C57BL/6J (female, 8 weeks old). $p53^{R172H/+}$ mice were continuously crossed with $BACH1^{-/-}$ mice to get $p53^{R172H/+}$ $BACH1^{-/-}$ mice. All mice were housed in rooms on a standard 12-h light–dark cycle, with a temperature range of 68–72 °F and humidity range of 30–70%. All animal experimental protocols were approved by the Institutional Animal Care and Use Committee of Columbia University. Mice would be killed if the tumor size/burden exceeded 1.5 cm in diameter; we confirm that the maximal tumor size/burden was not exceeded in this study.

## Tumor growth and tumor metastasis models

**Cal-33 xenograft model.** Cal-33 cells ($5 \times 10^5$) were mixed with Matrigel (Corning, cat. no. 354248) at a 1:1 ratio (v/v) and injected subcutaneously into Balb/c NU/NU nude mice (CAnN.Cg-Foxn1nu/Crl, 6 weeks old, female). Around 3 weeks later, mice were killed and tumors were weighed, imaged, subjected to western blot analysis, qPCR analysis, C11-BODIPY staining or IHC staining.

**HCT116 xenograft model.** HCT116 BACH1 inducible cells were made from HCT116 $BACH1^{-/-}$ cells by transfecting BACH1 inducible plasmid. HCT116 inducible cells were pre-incubated with or without doxycycline for 48 h in vitro and subcutaneously injected into Balb/c NU/NU nude mice (CAnN.Cg-Foxn1nu/Crl, 6 weeks old, female) and mice were fed with or without doxycycline diet (Envigo, cat. no. TD.01306, 625 mg doxycycline per kg rodent diet). Mice were killed at day 20 and the tumors were weighed, imaged and subjected to IHC staining.

**Tail vein injection lung metastasis model 1 (fluorescence system).** Cal-33 cells, mouse sarcoma cells, or HCT116 cells were transduced with dTomato (red fluorescence) lentivirus and sorted by FACS and then 0.5–4 million cells (for Cal-33 cells: 0.5–1 million per mouse; for mouse sarcoma cells: 1 million per mouse; for HCT116: 4 million per mouse) were injected into Balb/c NU/NU nude mice (CAnN.Cg-Foxn1nu/Crl, 6 weeks old, female) via tail vein. Six to eight weeks later, mice were killed and lungs were isolated for imaging using KEYENCE BZ-X800 fluorescence microscope. Lung metastases were quantified by KEYENCE BZ-X800 Analyzer. Then, lungs were fixed by 10% formalin and subjected to H&E staining and Ki67 IHC staining (Abcam, cat. no. ab16667).

**Tail vein injection lung metastasis model 2 (luciferase system).** Cal-33 cells were transduced with Tomato-luciferase lentivirus and sorted by FACS, followed by tail vein injection of those cells (0.5 million) into Balb/c NU/NU nude mice (CAnN.Cg-Foxn1nu/Crl, 6 weeks old, female). Four or three weeks later, mice were i.p. injected with luciferase substrate D-luciferin (PerkinElmer, cat. no.122799) and imaged on IVIS Spectrum Optical Imaging System.

## Western blotting and immunoprecipitation

Cells were lysed using RIPA buffer containing 10 mM Tris-Cl, pH 8.0, 150 mM NaCl, 1% Triton X-100, 1% Na-deoxycholate, 1 mM EDTA, 0.05% SDS and fresh 1× proteinase inhibitor. Protein concentration was determined by Protein Assay Dye Reagent (BIO-RAD, cat. no. 5000006) before samples were equally loaded and separated in SDS–PAGE gels. Proteins were then electro-transferred onto 0.45-μm nitrocellulose membranes (Thermo Fisher Scientific, cat. no. 88018) and incubated overnight at 4 °C or 1.5 h at room temperature with primary antibodies. HRP-conjugated secondary antibodies were used and western blot signals were detected on autoradiographic films after incubating with Pierce ECL Western Blotting Substrate (Thermo Fisher Scientific, cat. no. 32106) or SuperSignal West Dura Extended Duration Substrate (Thermo Fisher Scientific, cat. no. 34076).

For endogenous IP, cells were collected in 1% NP40 lysis buffer (1% NP40, 150 mM NaCl, 50 mM Tris-HCl and 1 mM EDTA) and incubated overnight with 4 μg IgG or p53 antibody (DO-1, Santa Cruz Biotechnology, cat. no. sc-126) followed by 4 h incubation with 0.1% BSA pre-blocked protein A agarose (GE Healthcare, cat. no. 17-0780-01).

Then, beads were washed with 1% NP40 lysis buffer and proteins were eluted with 0.1 M, pH 2.6, glycine for 15 min at room temperature. For SBP IP, cells were collected in 1% NP40 lysis buffer and incubated overnight with streptavidin beads (Thermo Fisher Scientific, cat. no. 45-000-279). Then, beads were washed with 1% NP40 lysis buffer and proteins were eluted with 2 mg ml$^{-1}$ biotin for 1 h at room temperature. For S-protein IP (second IP after SBP IP), protein elutes were incubated overnight with S-protein agarose (Millipore, cat. no. 69704). Then, beads were washed with 1% NP40 lysis buffer and proteins were eluted with 0.1 M, pH 2.6, glycine for 15 min at room temperature. Antibodies used are listed in Supplementary Table 2.

## Quantitative PCR

Total RNA was extracted using TRIzol (Thermo Fisher Scientific, cat. no. 15596018) according to the manufacturer's protocol. cDNA was generated using SuperScript IV VILO Master Mix (Thermo Fisher Scientific, cat. no. 11756500). Quantitative PCR was conducted using a 7500 Fast Real-Time PCR System (Applied Biosystems) with standard protocol. Reactions were performed in triplicate. Quantitative PCR primers are listed in Supplementary Table 3.

## RNAi interference and CRSIPR genome editing

Cells were plated at 20–30% density one day before siRNA transfection and then transfected with 80 nM siRNA pool using Lipofectamine 3000 (Thermo Fisher Scientific, cat. no. L3000008). Cells were collected at 48–72 h after transfection and subjected to functional assays. LSD2 siRNAs pool (Horizon Discovery, cat. no. L-008121-01-0005); p53 siRNAs pool (Horizon Discovery, cat. no. L-003329-00-0020); BACH1 siRNAs pool (Horizon Discovery, cat. no. L-007750-00-0020); non-targeting siRNAs pool (Horizon Discovery, cat. no. D-001810-10).

For CRISPR experiment, TrueGuide Synthetic gRNAs (Thermo Fisher Scientific, cat. no. A35533) were co-transfected with TrueCut Cas9 Protein v2 (Thermo Fisher Scientific, cat. no. A36498) into cells using Lipofectamine CRISPRMAX (Thermo Fisher Scientific, cat. no. CMAX00008) according to the manufacturer's protocol. Forty-eight hours later, CRISPR efficiency was determined by western blot analysis and then pool cells were seeded in 10-cm dish to grow clones at a density of 100–200 cells per dish. One or two weeks later, moloclones were picked and seeded into 12-well plates, followed by identification by western blot analysis. Oligonucleotides (siRNAs and gRNAs) used are listed in Supplementary Table 3.

## Chromatin immunoprecipitation assay

Cells were crosslinked with 1% formaldehyde for 10 min (for H3K4me2 ChIP, the fix time is 2–3 min) at room temperature and neutralized by adding glycine to a final concentration of 0.125 M. After twice washing with cold PBS, cells were collected and suspended in ChIP lysis buffer A (10 mM Tris-Cl, pH 8.0, 85 mM KCl, 0.5% NP40, 5 mM EDTA and 1× proteinase inhibitor). After 10 min incubation on ice, nuclei were collected and re-suspended in ChIP lysis buffer B (1% Triton X-100, 10 mM Tris-HCl, pH 8.0, 150 mM NaCl, 5 mM EDTA, 0.1% SDS, 0.1% sodium deoxycholate and 1× protease inhibitor) for 10 min at 4 °C. After sonication for 4 min, the lysates were centrifuged and the supernatants were collected and pre-cleaned by 0.1% BSA incubated protein A agarose (GE Healthcare, cat. no. 17-0780-01) for 1 h at 4 °C. The pre-cleaned lysates were aliquoted equally and incubated with indicated antibodies overnight at 4 °C. Protein A agarose was added into each sample and incubated for 2 h at 4 °C. The agarose was washed with TSE I (20 mM Tris-HCl, pH 8.0, 2 mM EDTA, 150 mM NaCl, 0.1% SDS and 1% Triton X-100), TSE II (20 mM Tris-HCl, pH 8.0, 2 mM EDTA, 500 mM NaCl, 0.1% SDS and 1% Triton X-100), buffer III (10 mM Tris-HCl, pH 8.0, 1 mM EDTA, 0.25 M LiCl, 1% DOC and 1% NP40) and buffer TE (10 mM Tris-HCl, pH 8.0, 1 mM EDTA), sequentially. The binding components were eluted in 1% SDS and 0.1 M NaHCO$_3$ and reverse cross-linkage was performed at 65 °C overnight. DNA was extracted using the PCR purification kit

(QIAGEN, 28106). qPCR was performed to detect relative enrichment of certain proteins on indicated gene promoters. ChIP qPCR primers are listed in Supplementary Table 3.

### Ferroptosis assays and C11-BODIPY staining

Cell death was determined using ToxiLight Non-destructive Cytotoxicity BioAssay kit (Lonza, cat. no. LT07-117) and some of results were double-confirmed by Trypan blue staining. Each treatment group had three cell culture replicates and each experiment was repeated three times. Data were collected using GloMax Explorer Multimode Microplate Reader (Promega). TBH (Sigma, cat. no. 458139) and erastin (Sigma, cat. no. 329600) were used to trigger ferroptosis by producing lipid ROS and inhibiting SLC7A11, respectively. Ferrostatin-1 (Xcess Biosciences, cat. no. M60042-10S) was used as a ferroptosis inhibitor.

For in vitro cultured cells staining, cells were treated with TBH for indicated time and incubated with BODIPY 581/591 C11 (Thermo Fisher Scientific, cat. no. D3861) at the concentration of 2.5 μM for 25–30 min at 37 °C in serum-free medium and then cells were washed with PBS, digested and washed with PBS again, followed by FACS analysis of lipid peroxidation level. The probe uptake was expressed as oxidized probe signal (excitation/emission 488/530 nm) over non-oxidized probe signal (excitation/emission 561/585 nm). For tumor-derived cells staining, tumor tissues were sliced and cut into small pieces and digested with 1 mg ml$^{-1}$ collagenase, type I (Thermo Fisher Scientific, cat. no. 17018029) for 1 h at 37 °C and then tissues were pipetted and filtered through syringe needles to obtain single cells. Cells were subjected to BODIPY 581/591 C11 staining for 25–30 min at room temperature in a rotator, followed by FACS analysis of lipid peroxidation level. FACS data were acquired with Attune NxT Acoustic Focusing Cytometer and FACS data were analyzed with FlowJo v.10.

### Lentivirus-based gene transfer

The 293T cells were transiently co-transfected with lentiviral backbone constructs (for example, pUltra-Chili dTomato and pHE3-Luc-tomato) and three packaging plasmids pLP1, pLP2 and pLP/VSV-G (or packaging plasmids, VSV-G and pCMV Delta R8.9) using the Lipofectamine 3000 transfection reagent (Thermo Fisher Scientific, cat. no. L3000008). Lentivirus-containing medium was collected at 48 h after transfection and supplemented with 8 μg ml$^{-1}$ polybrene (Sigma, cat. no. TR-1003). Cal-33 cells, sarcoma cells and HCT116 cells were infected by replacing the cell culture medium with lentivirus-containing medium and centrifuged at 580g for 1 h followed by 37 °C culture for 24 h. Stable cells were sorted by FACS using Tomoto fluorescence.

### Luciferase assays

A firefly reporter (SLC7A11-Luci reporter or SLC7A11-Luci mutant reporter) and a Renilla control reporter were co-transfected with indicated constructs in H1299 cells for 24 or 48 h and the relative luciferase activity was measured by dual-luciferase assay kit (Promega, cat. no. E1960). Dual-luciferase assay data were collected using GloMax Explorer Multimode Microplate Reader (Promega).

### Immunohistochemistry staining

Tumor or tissue samples were fixed in 10% formalin for 24 h and then transferred to 70% ethanol and subjected to standard dehydration processing for preparing the paraffin wax blocks. Paraffin blocks were sectioned at 4-μM thickness for H&E staining and IHC staining. The 4-HNE, SLC7A11 and Ki67 staining was quantified by the immunoreactive score system. The percentage of positive cells was scored as follows: no stained cells, 0; 1–10% staining, 1; 10–50% staining, 2; 51–80% staining, 3; and 81–100% staining, 4. The staining intensity was scored as follows: no color reaction, 0; mild reaction, 1; moderate reaction, 2; and intense reaction, 3. Final immunoreactive scores of immunohistochemistry = (scores of staining intensity) × (scores of percentage of positive cells).

### Statistics and reproducibility

Data were presented as means ± s.e.m., calculated by GraphPad Prism v.9.0 software. Unless otherwise stated, data were analyzed by two-tailed $t$-tests. $P$ values of survival curves were calculated by log-rank (Mantel–Cox) test. Differences were considered statistically significant if *$P < 0.05$, **$P < 0.01$ or ***$P < 0.001$. Statistical analyses were done with Excel v.2016 and GraphPad Prism v.9. No statistical method was used to predetermine sample size but our sample sizes are similar to those reported in previous publications[16,18]. No data were excluded from the analyses; Data distribution was assumed to be normal but this was not formally tested. Nude mice for xenograft and metastasis experiments were allocated randomly into each experimental group; in vitro experiments were not randomized. Data collection and analysis were not performed blind to the conditions of the experiments.

### Reporting summary

Further information on research design is available in the Nature Portfolio Reporting Summary linked to this article.

### Data availability

RNA-seq data from Cal-33 cells have been deposited to the Gene Expression Omnibus under accession code GSE224730. An analyzed result for this RNA-sequencing is available in Supplementary Table 1. Proteomics data have been deposited in ProteomeXchange via the PRIDE database, with a relevant accession number PXD039886. The human pan-cancer data were derived from the TCGA Research Network: http://cancergenome.nih.gov/ and cBioPortal: https://www.cbioportal.org/. The dataset derived from this resource that supports the findings of this study is available in Source Data Extended Data Fig. 10. Source Data for Figs. 1–8 and Extended Data Figs. 1–10 have been provided as Source Data files. All other data supporting the findings of this study are available from the corresponding author on reasonable request. Source data are provided with this paper.

### References

1. Schulz-Heddergott, R. & Moll, U. M. Gain-of-function (GOF) mutant p53 as actionable therapeutic target. *Cancers* **10**, 188 (2018).
2. Brosh, R. & Rotter, V. When mutants gain new powers: news from the mutant p53 field. *Nat. Rev. Cancer* **9**, 701–713 (2009).
3. Cho, Y., Gorina, S., Jeffrey, P. D. & Pavletich, N. P. Crystal structure of a p53 tumor suppressor-DNA complex: understanding tumorigenic mutations. *Science* **265**, 346–355 (1994).
4. Muller, P. A. & Vousden, K. H. Mutant p53 in cancer: new functions and therapeutic opportunities. *Cancer Cell* **25**, 304–317 (2014).
5. Tang, Q., Su, Z., Gu, W. & Rustgi, A. K. Mutant p53 on the path to metastasis. *Trends Cancer* **6**, 62–73 (2020).
6. Cooks, T. et al. Mutant p53 prolongs NF-κB activation and promotes chronic inflammation and inflammation-associated colorectal cancer. *Cancer Cell* **23**, 634 (2013).
7. Muller, P. A. et al. Mutant p53 drives invasion by promoting integrin recycling. *Cell* **139**, 1327–1341 (2009).
8. Zhu, J. et al. Gain-of-function p53 mutants co-opt chromatin pathways to drive cancer growth. *Nature* **525**, 206–211 (2015).
9. Weissmueller, S. et al. Mutant p53 drives pancreatic cancer metastasis through cell-autonomous PDGF receptor β signaling. *Cell* **157**, 382–394 (2014).
10. Freed-Pastor, W. A. et al. Mutant p53 disrupts mammary tissue architecture via the mevalonate pathway. *Cell* **148**, 244–258 (2012).
11. Schulz-Heddergott, R. et al. Therapeutic ablation of gain-of-function mutant p53 in colorectal cancer inhibits Stat3-mediated tumor growth and invasion. *Cancer Cell* **34**, 298–314 (2018).

12. Escobar-Hoyos, L. F. et al. Altered RNA splicing by mutant p53 activates oncogenic RAS signaling in pancreatic cancer. *Cancer Cell* **38**, 198–211 (2020).

13. Girardini, J. E. et al. A Pin1/mutant p53 axis promotes aggressiveness in breast cancer. *Cancer Cell* **20**, 79–91 (2011).

14. Adorno, M. et al. A mutant-p53/Smad complex opposes p63 to empower TGF-β-induced metastasis. *Cell* **137**, 87–98 (2009).

15. Tang, Q. et al. Rab11-FIP1 mediates epithelial–mesenchymal transition and invasion in esophageal cancer. *EMBO Rep.* **22**, e48351 (2021).

16. Tang, Q. et al. Mutant p53 regulates Survivin to foster lung metastasis. *Genes Dev.* **35**, 528–541 (2021).

17. Hanel, W. et al. Two hot spot mutant p53 mouse models display differential gain of function in tumorigenesis. *Cell Death Diff.* **20**, 898–909 (2013).

18. Olive, K. P. et al. Mutant p53 gain of function in two mouse models of Li-Fraumeni syndrome. *Cell* **119**, 847–860 (2004).

19. Lang, G. A. et al. Gain of function of a p53 hot spot mutation in a mouse model of Li-Fraumeni syndrome. *Cell* **119**, 861–872 (2004).

20. Bougeard, G. et al. Revisiting Li-Fraumeni syndrome from TP53 mutation carriers. *J. Clin. Oncol.* **33**, 2345–2352 (2015).

21. Davudian, S., Mansoori, B., Shajari, N., Mohammadi, A. & Baradaran, B. BACH1, the master regulator gene: a novel candidate target for cancer therapy. *Gene* **588**, 30–37 (2016).

22. Sun, J. et al. Hemoprotein Bach1 regulates enhancer availability of heme oxygenase-1 gene. *EMBO J.* **21**, 5216–5224 (2002).

23. Lee, J. et al. Effective breast cancer combination therapy targeting BACH1 and mitochondrial metabolism. *Nature* **568**, 254–258 (2019).

24. Ying, Y. et al. Oncogenic HOXB8 is driven by MYC-regulated super-enhancer and potentiates colorectal cancer invasiveness via BACH1. *Oncogene* **39**, 1004–1017 (2020).

25. Sato, M. et al. BACH1 promotes pancreatic cancer metastasis by repressing epithelial genes and enhancing epithelial–mesenchymal transitionaddiction of pancreatic cancer to BACH1 in EMT. *Cancer Res.* **80**, 1279–1292 (2020).

26. Nishizawa, H. et al. Ferroptosis is controlled by the coordinated transcriptional regulation of glutathione and labile iron metabolism by the transcription factor BACH1. *J. Biol. Chem.* **295**, 69–82 (2020).

27. Wiel, C. et al. BACH1 stabilization by antioxidants stimulates lung cancer metastasis. *Cell* **178**, 330–345 (2019).

28. Lignitto, L. et al. Nrf2 activation promotes lung cancer metastasis by inhibiting the degradation of Bach1. *Cell* **178**, 316–329 (2019).

29. Liang, Y. et al. Transcriptional network analysis identifies BACH1 as a master regulator of breast cancer bone metastasis. *J. Biol. Chem.* **287**, 33533–33544 (2012).

30. Wang, D. et al. Acetylation-regulated interaction between p53 and SET reveals a widespread regulatory mode. *Nature* **538**, 118–122 (2016).

31. Maddika, S. et al. WWP2 is an E3 ubiquitin ligase for PTEN. *Nat. Cell Biol.* **13**, 728–733 (2011).

32. Meitinger, F. et al. 53BP1 and USP28 mediate p53 activation and G1 arrest after centrosome loss or extended mitotic duration. *J. Cell Biol.* **214**, 155–166 (2016).

33. Inoue, K., Fry, E. A. & Frazier, D. P. Transcription factors that interact with p53 and M dm2. *Int. J. Cancer* **138**, 1577–1585 (2016).

34. Luo, J. et al. Negative control of p53 by Sir2α promotes cell survival under stress. *Cell* **107**, 137–148 (2001).

35. Jiang, L. et al. Ferroptosis as a p53-mediated activity during tumour suppression. *Nature* **520**, 57–62 (2015).

36. Jennis, M. et al. An African-specific polymorphism in the TP53 gene impairs p53 tumor suppressor function in a mouse model. *Genes Dev.* **30**, 918–930 (2016).

37. Stockwell, B. R., Jiang, X. & Gu, W. Emerging mechanisms and disease relevance of ferroptosis. *Trends Cell Biol.* **30**, 478–490 (2020).

38. Chu, B. et al. ALOX12 is required for p53-mediated tumour suppression through a distinct ferroptosis pathway. *Nat. Cell Biol.* **21**, 579–591 (2019).

39. Yang, W. S. et al. Regulation of ferroptotic cancer cell death by GPX4. *Cell* **156**, 317–331 (2014).

40. Warnatz, H.-J. et al. The BTB and CNC homology 1 (BACH1) target genes are involved in the oxidative stress response and in control of the cell cycle. *J. Biol. Chem.* **286**, 23521–23532 (2011).

41. Rodrigues, G. et al. Tumour exosomal CEMIP protein promotes cancer cell colonization in brain metastasis. *Nat. Cell Biol.* **21**, 1403–1412 (2019).

42. Zhang, C. et al. FABP5 promotes lymph node metastasis in cervical cancer by reprogramming fatty acid metabolism. *Theranostics* **10**, 6561 (2020).

43. Nam, S. W. et al. Autotaxin (NPP-2), a metastasis-enhancing motogen, is an angiogenic factor. *Cancer Res.* **61**, 6938–6944 (2001).

44. Sjöberg, E. et al. A novel ACKR2-dependent role of fibroblast-derived CXCL14 in epithelial-to-mesenchymal transition and metastasis of breast cancer. *Clin. Cancer Res.* **25**, 3702–3717 (2019).

45. Zhao, L. et al. KIAA1199 promotes metastasis of colorectal cancer cells via microtubule destabilization regulated by a PP2A/stathmin pathway. *Oncogene* **38**, 935–949 (2019).

46. Rashid, O. M. et al. Is tail vein injection a relevant breast cancer lung metastasis model? *J. Thorac. Dis.* **5**, 385 (2013).

47. Ota, K., Brydun, A., Itoh-Nakadai, A., Sun, J. & Igarashi, K. Bach1 deficiency and accompanying overexpression of heme oxygenase-1 do not influence aging or tumorigenesis in mice. *Oxid. Med. Cell. Longev.* **2014**, 757901 (2014).

48. Lan, F., Nottke, A. C. & Shi, Y. Mechanisms involved in the regulation of histone lysine demethylases. *Curr. Opin. Cell Biol.* **20**, 316–325 (2008).

49. Ciccone, D. N. et al. KDM1B is a histone H3K4 demethylase required to establish maternal genomic imprints. *Nature* **461**, 415–418 (2009).

50. Fang, R. et al. Human LSD2/KDM1b/AOF1 regulates gene transcription by modulating intragenic H3K4me2 methylation. *Mol. Cell* **39**, 222–233 (2010).

51. Fang, R. et al. LSD2/KDM1B and its cofactor NPAC/GLYR1 endow a structural and molecular model for regulation of H3K4 demethylation. *Mol. Cell* **49**, 558–570 (2013).

52. Beischlag, T. V., Prefontaine, G. G. & Hankinson, O. ChIP-re-ChIP: co-occupancy analysis by sequential chromatin immunoprecipitation. *Methods Mol. Biol.* **1689**, 103–112 (2018).

53. Dohi, Y. et al. Bach1 inhibits oxidative stress-induced cellular senescence by impeding p53 function on chromatin. *Nat. Struct. Mol. Biol.* **15**, 1246–1254 (2008).

54. Liu, D. S. et al. Inhibiting the system xC–/glutathione axis selectively targets cancers with mutant-p53 accumulation. *Nat. Commun.* **8**, 1–14 (2017).

55. Kumar, A. et al. Expression profile of H3K4 demethylases with their clinical and pathological correlation in patients with clear cell renal cell carcinoma. *Gene* **739**, 144498 (2020).

56. Katz, T. A. et al. Inhibition of histone demethylase, LSD2 (KDM1B), attenuates DNA methylation and increases sensitivity to DNMT inhibitor-induced apoptosis in breast cancer cells. *Breast Cancer Res. Treat.* **146**, 99–108 (2014).

57. Burg, J. M. et al. KDM1 class flavin-dependent protein lysine demethylases. *Pept. Sci.* **104**, 213–246 (2015).

## Author contributions

Conception and experimental design was the responsibility of Z.S. and W.G. Methodology and data acquisition was the responsibility of Z.S., N.K., J.Y., Z.L., H.L. and Y.L. Analysis and interpretation of data was carried out by Z.S., N.K., H.Z., W.Z., Q.T., H.K., K.O., S.D., Z. Z., B.H., A.R., J. M. and W.G. Manuscript writing was the responsibility of Z.S. and W.G.

## Competing interests

The authors declare no competing interests.

## Additional information

**Extended data** is available for this paper at https://doi.org/10.1038/s43018-023-00532-z.

**Supplementary information** The online version contains supplementary material available at https://doi.org/10.1038/s43018-023-00532-z.

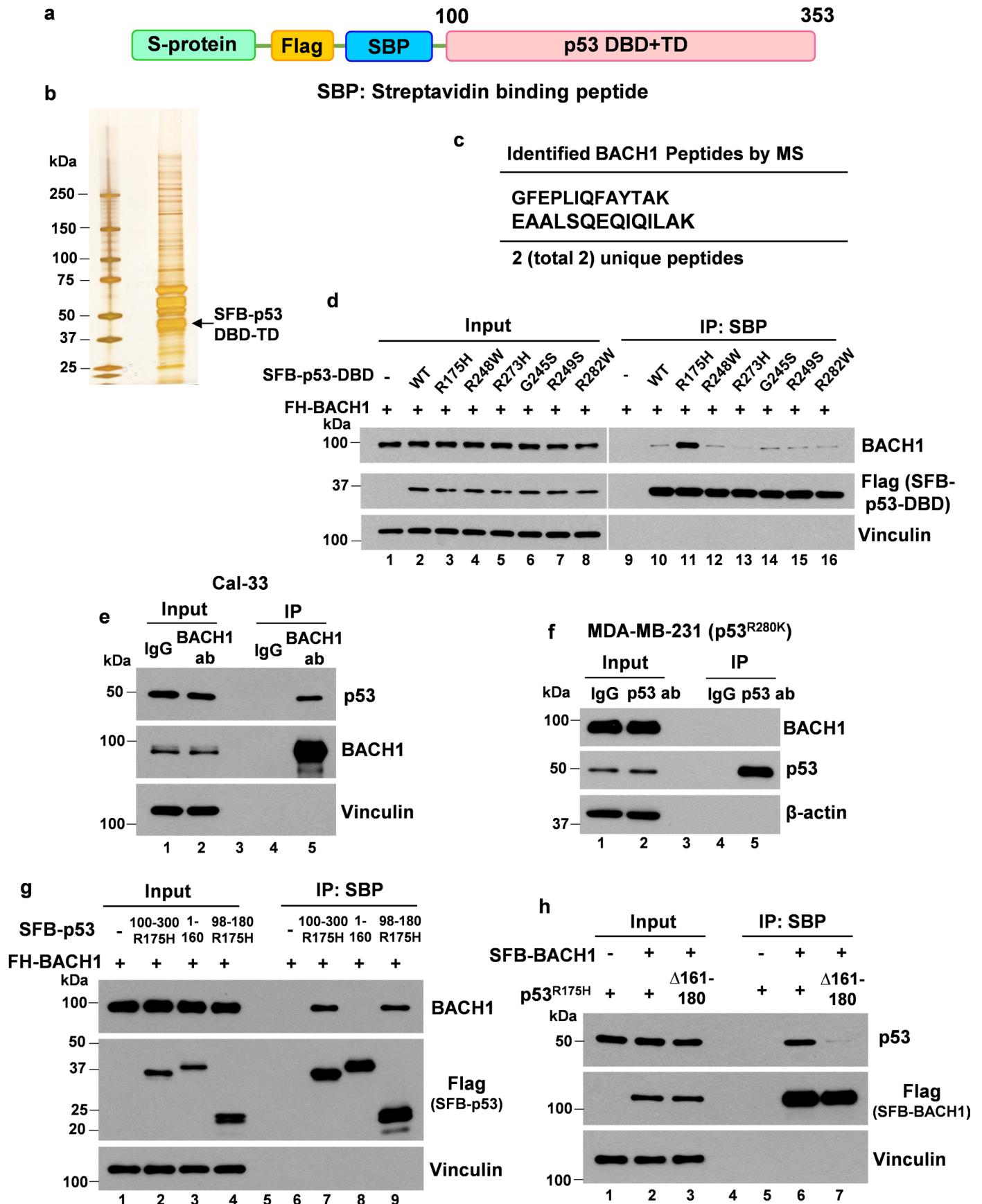**Correspondence and requests for materials** should be addressed to Wei Gu.

**Peer review information** *Nature Cancer* thanks Scott Dixon, Kazuhiko Igarashi and the other, anonymous, reviewer(s) for their contribution to the peer review of this work.

**Reprints and permissions information** is available at www.nature.com/reprints.

**a**

S-protein — Flag — SBP — (100) — p53 DBD+TD (353)

SBP: Streptavidin binding peptide

**b**

SFB-p53 DBD-TD

**c** Identified BACH1 Peptides by MS

GFEPLIQFAYTAK
EAALSQEQIQILAK

2 (total 2) unique peptides

**d** Input | IP: SBP

**e** Cal-33

**f** MDA-MB-231 (p53$^{R280K}$)
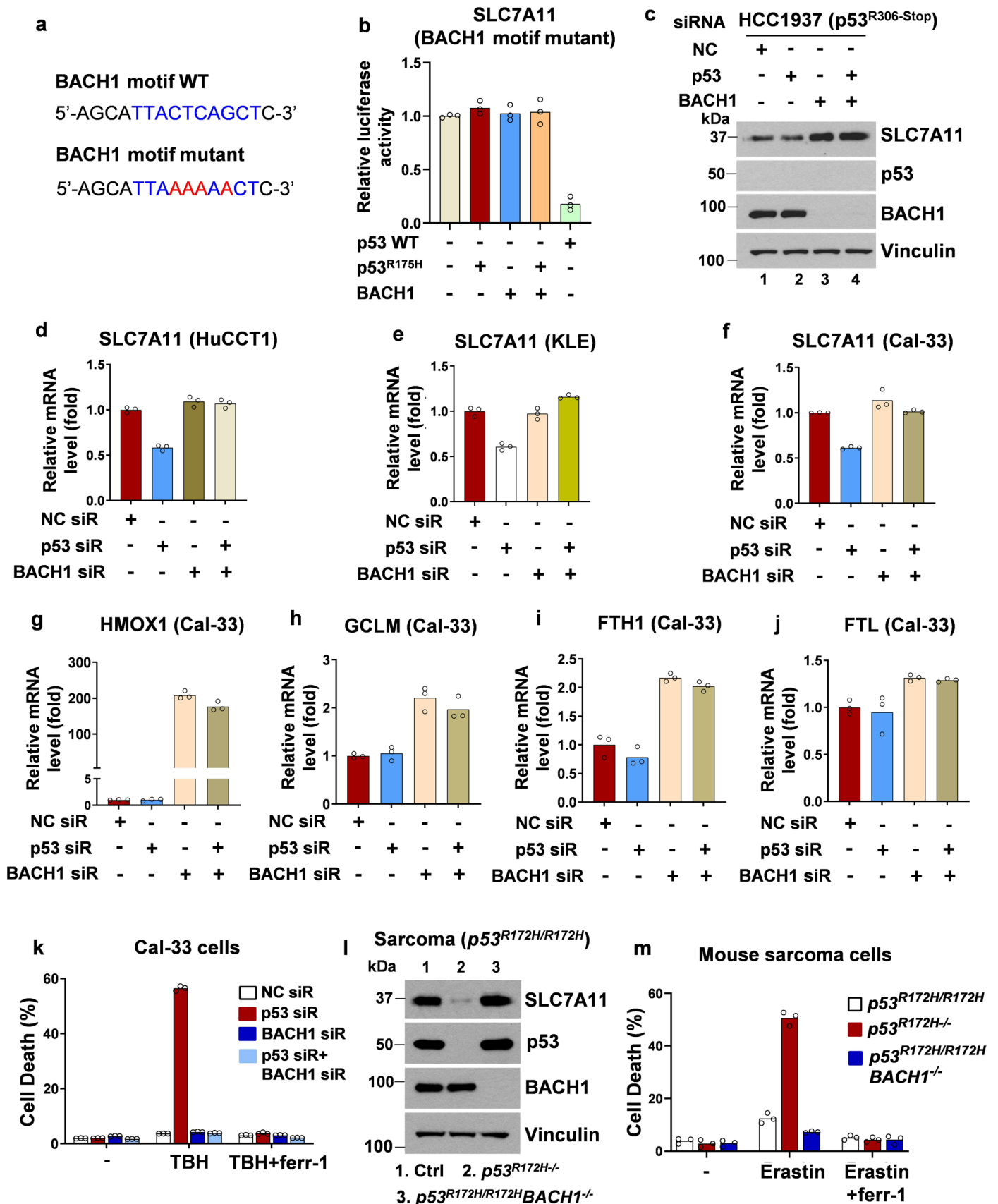
**g** Input | IP: SBP

**h** Input | IP: SBP

Extended Data Fig. 1 | See next page for caption.

**Extended Data Fig. 1 | Identification of BACH1 as a specific binding partner of p53$^{R175H}$. a**, Diagram of the construct of SFB-tagged wild-type p53 DBD + TD domains. DBD, DNA binding domain; TD, tetramerization domain; SFB tag: S-protein, Flag and streptavidin binding peptide (SBP). **b**, Silver staining of SDS−PAGE gel loaded with SFB-p53 DBD + TD protein complex purified from H1299 cell line stably overexpressing SFB-p53 DBD + TD protein by double IP (SBP IP + S-protein IP). **c**, BACH1 peptides sequences identified from Mass-Spec of p53 DBD + TD protein complex. **d**, Co-IP of SFB-tagged p53 DBD (WT, R175H, R248W, R273H, G245S, R249S and R282W) with Flag-HA (FH)-BACH1. H1299 p53 null cells were co-transfected with SFB-tagged p53 DBD and FH-BACH1 and 24 h later,

cells were lysed with NP40 lysis buffer and immunoprecipitated with SBP beads, followed by Western blot analysis of BACH1 and Flag (SFB-p53). **e**, p53$^{R175H}$-BACH1 endogenous Co-IP by BACH1 specific antibody in Cal-33 cells. **f**, Endogenous co-IP of p53 and BACH1 in mutant p53 cell lines MDA-MB-231 (p53$^{R280K}$). **g**, Co-IP of SFB-tagged p53$^{R175H}$ truncated domains (100-300-R175H, 1-160 and 98-180-R175H) with Flag-HA (FH)-BACH1 in H1299 cells. **h**, Co-IP of SFB-tagged BACH1 with p53$^{R175H}$ and its deletion mutant (Δ161-180 aa) in H1299 cells. SFB, S-protein-Flag-Streptavidin binding peptide; SBP, streptavidin binding peptide. Gel staining (b) and Western blot experiments (d-h) were repeated three times with similar results and representative images are shown.
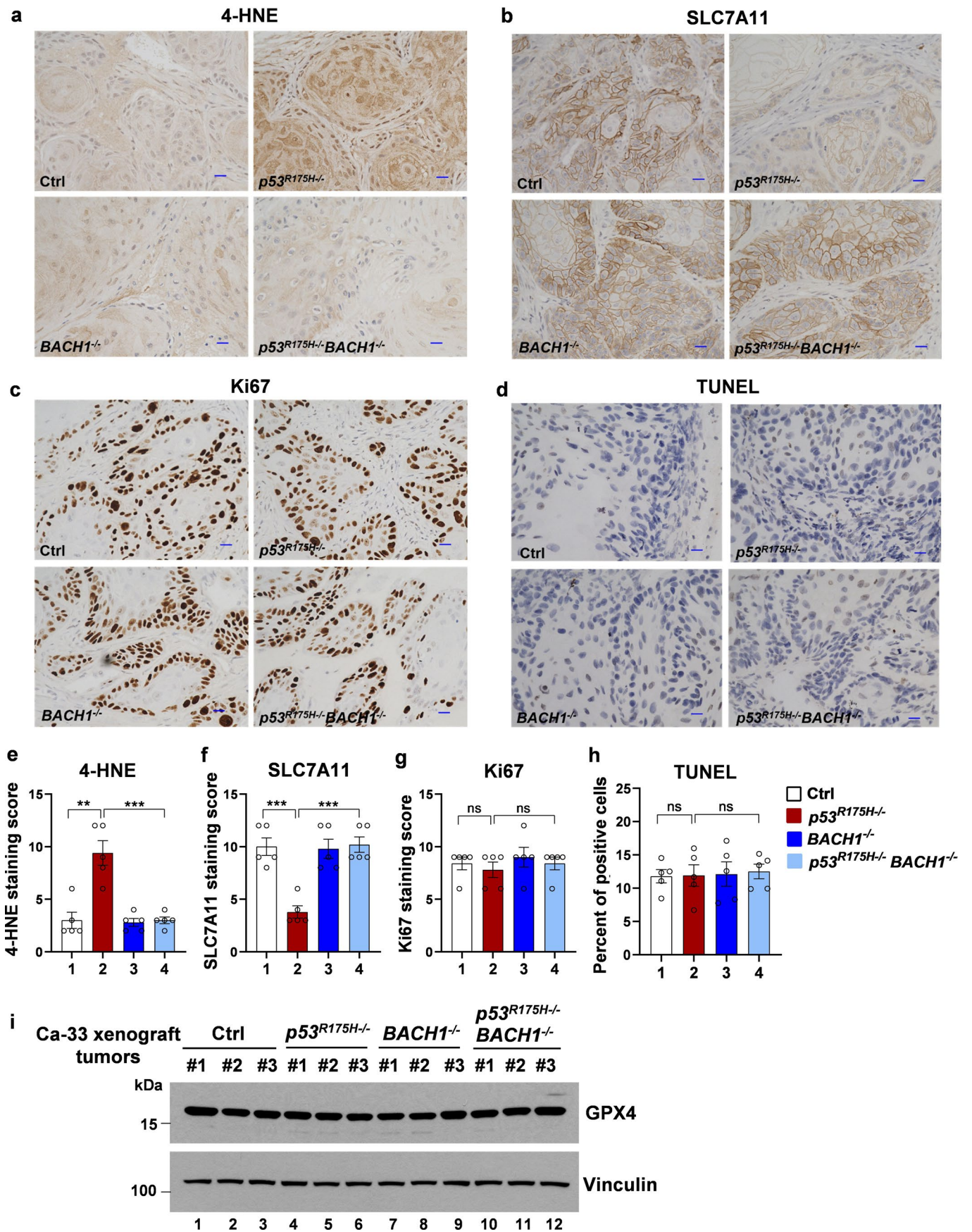
**a**

**BACH1 motif WT**

5'-AGCATTACTCAGCTC-3'

**BACH1 motif mutant**

5'-AGCATTAAAAAACTC-3'

**b** SLC7A11 (BACH1 motif mutant)

**c** siRNA HCC1937 (p53$^{R306-Stop}$)

**d** SLC7A11 (HuCCT1)

**e** SLC7A11 (KLE)

**f** SLC7A11 (Cal-33)

**g** HMOX1 (Cal-33)

**h** GCLM (Cal-33)

**i** FTH1 (Cal-33)

**j** FTL (Cal-33)

**k** Cal-33 cells

**l** Sarcoma (p53$^{R172H/R172H}$)

1. Ctrl    2. p53$^{R172H-/-}$

3. p53$^{R172H/R172H}$BACH1$^{-/-}$

**m** Mouse sarcoma cells

Extended Data Fig. 2 | See next page for caption.

**Extended Data Fig. 2 | p53$^{R175H}$ suppresses BACH1-mediated transcriptional regulation of SLC7A11 and ferroptosis. a**, SLC7A11 promoter sequences containing the BACH1 consensus binding motif (WT or mutated; -118 to -127bp). Wild-type or mutant SLC7A11 promoters were cloned into the pGL3 luciferase reporter vector. **b**, Dual-luciferase reporter assay for SLC7A11 transcription in H1299 cells co-transfected with control, p53-R175H, BACH1, p53-R175H + BACH1, or WT p53 plasmid, along with SLC7A11 luciferase reporter plasmid (containing mutant motif) and Renilla plasmid. n = 3 technical cell culture replicates. The experiment was repeated three times with similar results. **c**, Western blot analysis of SLC7A11 expression in HCC1937 cells (p53$^{R306-stop}$) treated with NC siRNA, p53 siRNA, BACH1 siRNA, or p53 siRNA+BACH1 siRNA for 48 h. The experiment was repeated twice with similar results. **d-f**, qPCR analysis of SLC7A11 mRNA expression in HuCCT1 cells (**d**), KLE cells (**e**) and Cal-33 cells (**f**) treated with NC siRNA, p53 siRNA, BACH1 siRNA, or p53 siRNA+BACH1 siRNA for 48-72 h. HuCCT1 cells, 48 h; KLE cells, 56 h; Cal-33 cells, 72 h. n = 3 technical replicates. The experiments were repeated twice with similar results. **g-j**, qPCR analysis of BACH1 targets in Cal-33 cells treated with NC siRNA, p53 siRNA, BACH1 siRNA, or p53 siRNA+BACH1 siRNA for 72 h. HMOX1 (**g**); GCLM (**h**); FTH1 (**i**); FTL (**j**). n = 3 technical replicates. The experiment was repeated twice with similar results. **k**, Cell death assay of Cal-33 NC, p53, BACH1, or p53 + BACH1 knockdown cells treated with 1 mM TBH for 8 h in presence or absence of 5 μM ferr-1. n = 3 technical cell culture replicates. The experiment was repeated three times with similar results. **l**, Western blot analysis of SLC7A11, p53 and BACH1 expression in mouse sarcoma cells. p53$^{R172H/R172H}$ sarcoma cell were from spontaneously-developed sarcoma tumors derived from p53$^{R172H/R172H}$ mice and p53$^{R172H/-}$ and p53$^{R172H/R172H}$BACH1$^{-/-}$ cells were made from these p53$^{R172H/R172H}$ cells by CRSIPR method. The experiment was repeated twice with similar results. **m**, Cell death assay for p53$^{R172H/R172H}$, p53$^{R172H/-}$ and p53$^{R172H/R172H}$BACH1$^{-/-}$ sarcoma cells treated with 0.5 μM erastin for 18 h in the presence or absence of 5 μM ferr-1. n = 3 technical cell culture replicates. The experiment was repeated three times with similar results. Data represent mean of three technical replicates.

**a** 4-HNE

**b** SLC7A11

**c** Ki67

**d** TUNEL

**e** 4-HNE

**f** SLC7A11

**g** Ki67

**h** TUNEL

Ctrl
$p53^{R175H-/-}$
$BACH1^{-/-}$
$p53^{R175H-/-}\ BACH1^{-/-}$

**i** Ca-33 xenograft tumors

**Extended Data Fig. 3 | See next page for caption.**

**Extended Data Fig. 3 | Immunohistochemical (IHC) staining and Western blot analysis of Cal-33 xenograft tumors. a-d**, IHC staining for 4-HNE (**a**), SLC7A11 (**b**), Ki67 (**c**) and TUNEL (**d**). Bar scale=20 μm. **e-h**, Quantification for 4-HNE (**e**), SLC7A11 (**f**), Ki67 (**g**) and TUNEL (**h**) staining. n = 5 fields from 5 tumors (each group). *P* values in e (from left to right): 0.0018; 0.0007. *P* values in f (from left to right): 0.0003; 0.0001. *P* values in g (from left to right): 0.5447; 0.5447. *P* values in h (from left to right): 0.9505; 0.7634. **i**, Western blot analysis of GPX4 expression. n = 3 tumor samples for each genotype. 4-HNE, SLC7A11 and Ki67 IHC staining was quantified by using the immunoreactive score (IRS) system and TUNEL staining were quantified with percentage of positive cells (see Methods for details). Two-tailed Student's t-test were used for statistical analysis. ns, not significant, **$p < 0.01$; ***$p < 0.001$. Data represent mean + S.E.M.
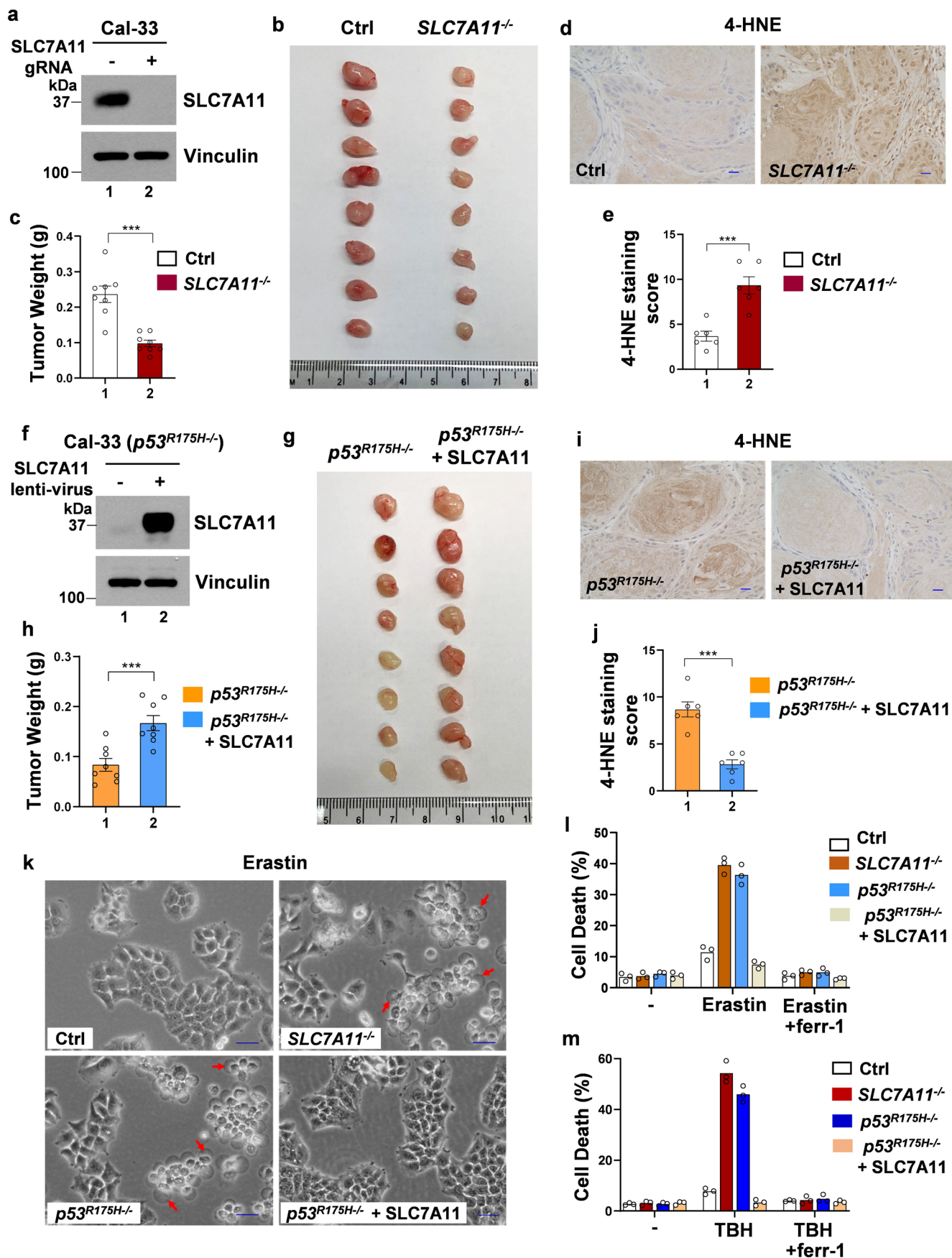
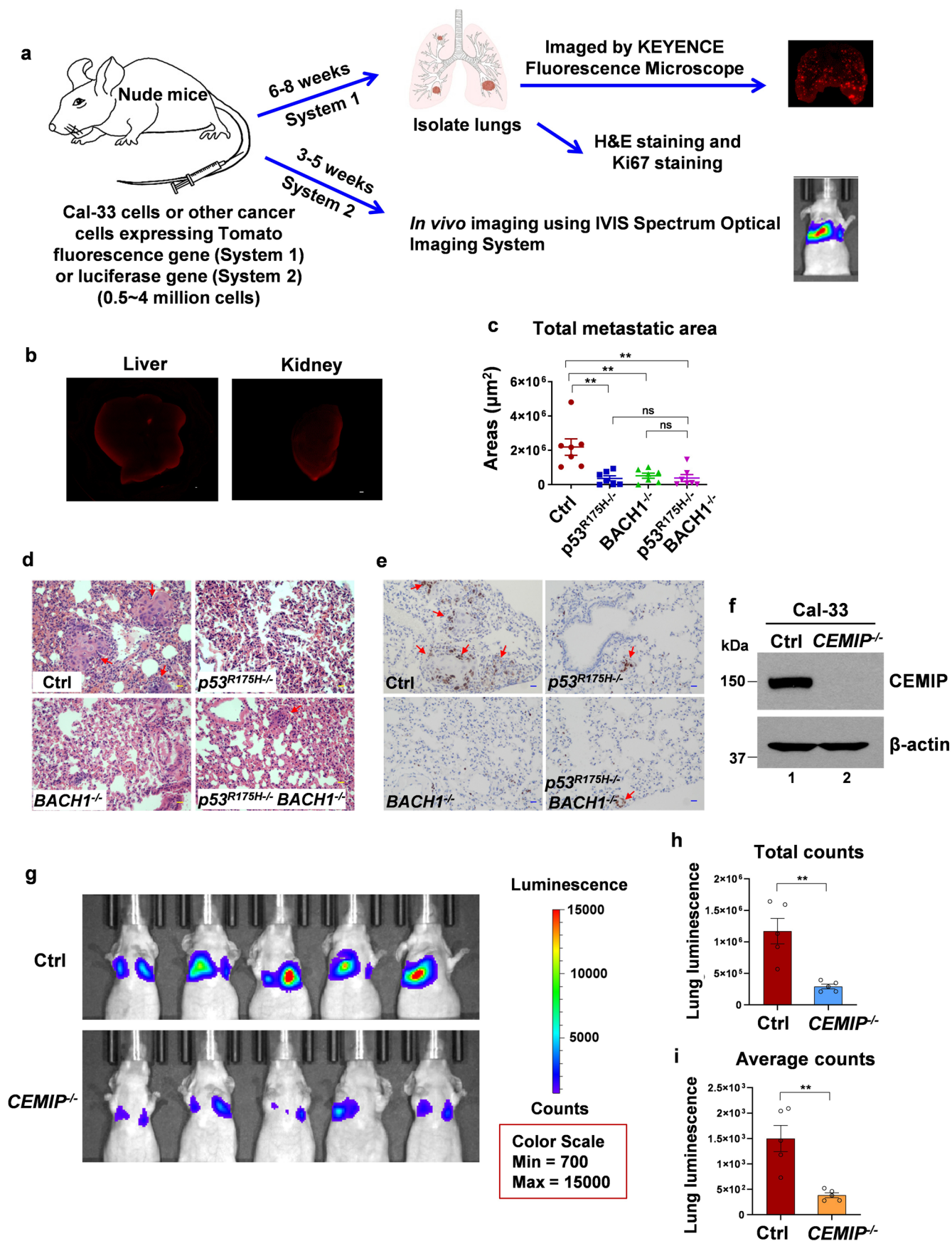**Extended Data Fig. 4 | See next page for caption.**

**Extended Data Fig. 4 | The role of SLC7A11 in p53$^{R175H}$-mediated inhibition of ferroptosis and promotion of tumor growth. a**, Identification of *SLC7A11$^{-/-}$* Cal-33 cells by Western blot analysis. **b**, Images of tumors isolated from nude mice implanted with Cal-33 Ctrl and *SLC7A11$^{-/-}$* cells. n = 8 tumors. **c**, Tumor weights for Cal-33 Ctrl and *SLC7A11$^{-/-}$* xenografts. n = 8 tumors. *P* value: <0.0001. **d**, Representative images of 4-HNE staining of Cal-33 Ctrl and *SLC7A11$^{-/-}$* xenograft tumors. Bar scale=20 μm. **e**, Quantification of 4-HNE staining using the immunoreactive score (IRS) system (n = 6 fields from 6 tumors). *P* value: 0.0004. **f**, Identification of *p53$^{R175H/-}$* SLC7A11 overexpressing Cal-33 cells by Western blot analysis. *p53$^{R175H/-}$* SLC7A11 overexpressing Cal-33 cells were made by transducing plenti6-SLC7A11/xCT-V5 lentivirus into *p53$^{R175H/-}$* cells. **g**, Images of tumors isolated from nude mice implanted with Cal-33 *p53$^{R175H/-}$* and *p53$^{R175H/-}$* +SLC7A11 cells. n = 8 tumors. **h**, Tumor weights for Cal-33 *p53$^{R175H/-}$* and *p53$^{R175H/-}$* +SLC7A11 xenografts. n = 8 tumors. *P* value: 0.0008. **i**, Representative images of 4-HNE staining of Cal-33 *p53$^{R175H/-}$* and *p53$^{R175H/-}$* +SLC7A11 xenograft tumors. Bar scale=20 μm. **j**, Quantification of 4-HNE staining using the IRS system (n = 6 fields from 6 tumors). *P* value: <0.0001. **k**, Representative images of ferroptotic cell death in Cal-33 Ctrl, *SLC7A11$^{-/-}$*, *p53$^{R175H/-}$* and *p53$^{R175H/-}$*+ SLC7A11 cells treated with 10 μM erastin for 72 h. Red arrows indicate cells undergoing ferroptotic cell death. Bar scale=50 μm. The images shown are representative of 3 repeats with similar results. **l**, Cell death assay for Cal-33 Ctrl, *SLC7A11$^{-/-}$*, *p53$^{R175H/-}$* and *p53$^{R175H/-}$* + SLC7A11 cells treated with 10 μM erastin for 72 h in presence or absence of 5 μM ferr-1. n = 3 technical cell culture replicates. The experiment was repeated three times with similar results. **m**, Cell death assay for Cal-33 Ctrl, *SLC7A11$^{-/-}$*, *p53$^{R175H/-}$* and *p53$^{R175H/-}$*+SLC7A11 cells treated with 0.85 mM TBH for 7 h in presence or absence of 5 μM ferr-1. n = 3 technical cell culture replicates. The experiment was repeated three times with similar results. Two-tailed Student's t-test were used for statistical analysis. ***p < 0.001; Data (l, m) represent mean of three technical replicates. Data (c, e, h and j) represent mean + S.E.M.

**Extended Data Fig. 5 | BACH1/p53$^{R175H}$–mediated regulation of CEMIP expression is critical for lung metastasis. a**, Diagram of lung metastasis models by tail vein injection in nude mice. Cal-33 cells or other cancer cells were transduced with Tomato fluorescence gene lentivirus (system 1) or luciferase-Tomato lentivirus (system 2) and sorted by FACS and then 0.5-4 million cells (dependent on cell type) were tail vein injected into each mouse. For system 1, 6-8 weeks later, mice were sacrificed and lungs were isolated for imaging using KEYENCE BZ-X800 fluorescence microscope. For system 2, 3-5 weeks later, mice were i.p. injected with luciferase substrate D-luciferin and imaged on IVIS Spectrum Optical Imaging System. **b**, Representative fluorescence images of liver and kidney isolated from mice tail vein injected with Cal-33 Ctrl cells, related to main Fig. 5a. Scale bar, 500μm. **c**, Quantitative analysis of total metastatic area (μm$^2$) in lungs, related to main Fig. 5a. n = 7 mice for each group. *P* values (from left to right): 0.0035; 0.0062; 0.0048; 0.9274; 0.6024. **d**, H&E staining of lung tissues infiltrated with Cal-33 cells, related to main Fig. 5a. Red arrows indicate the metastatic nodes; panel d is a representative image of 5 lung sections from 5 mice (each group). Bar scale=20 μm. **e**, Immunohistochemical staining of Ki67 of lung tissues infiltrated with Cal-33 cells, related to main Fig. 5a. Red arrows indicate the Ki67 positive cell clusters; panel e is a representative image of 5 lung sections from 5 mice (each group). Bar scale=20 μm. **f**, Identification of *CEMIP$^{-/-}$* Cal-33 cells made by CRISPR method. **g**, In vivo luminescence imaging of mice 4 weeks after tail vein injection of 0.5 million of luciferase carrying Cal-33 Ctrl or *CEMIP$^{-/-}$* cells. Mice were imaged on IVIS System. n = 5 mice for each group. **h, i**, Quantitative analysis of total counts of luminescence (**h**) and average counts of luminescence (**i**) in lungs, related to panel (g). n = 5 mice for each group. *P* value (h): 0.0027. *P* value (i): 0.0028. Two-tailed Student's t-test were used for statistical analysis. ns, not significant, **p < 0.01; Data represent mean + S.E.M.
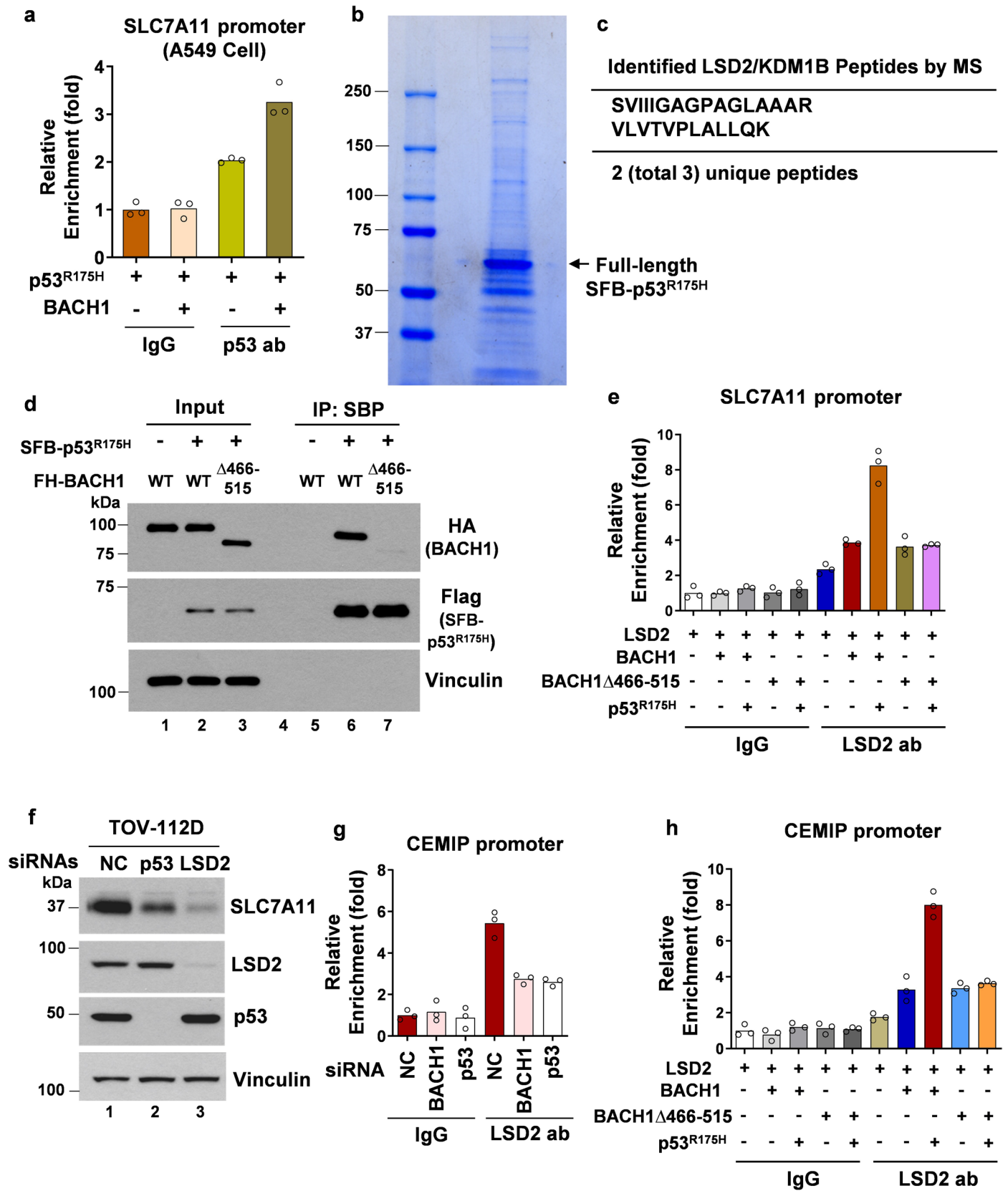
**a**



**b**



**c**



**d**



**e**



**f**
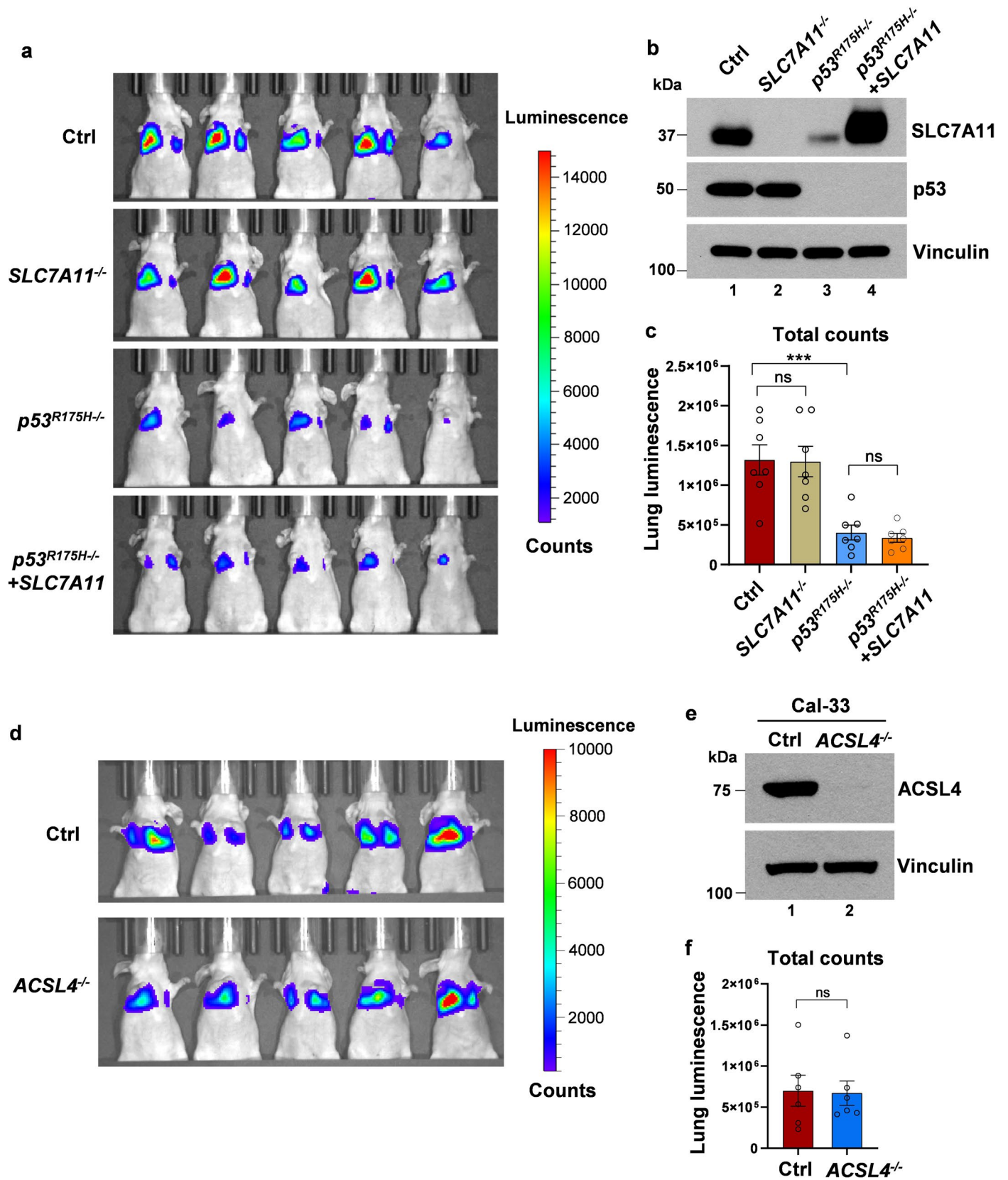


**Extended Data Fig. 6 | See next page for caption.**

**Extended Data Fig. 6 | The role of SLC7A11 and ACSL4 in lung metastasis of Cal-33 cells. a**, In vivo luminescence imaging of mice 4 weeks after tail vein injection of 0.5 million of luciferase carrying Cal-33 cells. $SLC7A11^{-/-}$ Cal-33 cells were made by CRISPR method and SLC7A11 overexpressing cells were made by transduction of SLC7A11 lentivirus into Cal-33 $p53^{R175H-/-}$ cells. Mice were i.p. injected with luciferase substrate D-luciferin and imaged on IVIS Spectrum Optical Imaging System. **b**, Western blot analysis of SLC7A11 and p53 expression in the above cell lines. b was repeated three times with similar results and a representative result is shown. **c**, Quantitative analysis of total counts of luminescence in lungs for each group, related to panel (a). n = 7 mice

for each group. *P* values (from left to right): 0.9398; 0.00097; 0.5446. **d**, In vivo luminescence imaging of mice 3 weeks after tail vein injection of 0.5 million of luciferase carrying control or $ACSL4^{-/-}$ Cal-33 cells. $ACSL4^{-/-}$ Cal-33 cells were made by CRISPR method. Mice were i.p. injected with luciferase substrate D-luciferin and imaged on IVIS Spectrum Optical Imaging System. **e**, Western blot analysis of ACSL4 expression in the above cell lines. e was repeated three times with similar results and a representative result is shown. **f**, Quantitative analysis of total counts of luminescence in lungs for each group, related to panel (d). n = 6 mice for each group. *P* value: 0.9049. Two-tailed Student's t-test were used for statistical analysis. ns, not significant, ***$p$ < 0.001; Data represent mean + S.E.M.

**c**

**Identified LSD2/KDM1B Peptides by MS**

SVIIIGAGPAGLAAAR
VLVTVPLALLQK

**2 (total 3) unique peptides**

**Extended Data Fig. 7 | See next page for caption.**

**Extended Data Fig. 7 | p53$^{R175H}$ regulates BACH1 targets through recruiting LSD2. a**, ChIP analysis of the recruitment of p53$^{R175H}$ to SLC7A11 promoter (-128 to -114) in A549 *p53*$^{-/-}$ cells transfected with p53$^{R175H}$ alone or p53$^{R175H}$ + BACH1 plasmids. n = 3 technical replicates. The experiment was repeated twice with similar results. **b**, Coomassie blue staining of SDS–PAGE gel loaded with SFB-p53$^{R175H}$ protein complex purified from H1299 cells stably expressing SFB-p53$^{R175H}$ by double IP (SBP IP + S-protein IP). The experiment was repeated three times with similar results. **c**, LSD2/KDM1B peptides sequences identified from Mass-Spec of SFB-p53$^{R175H}$ complex. **d**, Co-IP of SFB-tagged p53$^{R175H}$ with Flag-HA (FH)-tagged BACH1 or its deletion mutant Δ466-515 in H1299 cells. The experiment was repeated three times with similar results. **e**, ChIP analysis with LSD2 antibody in Cal-33 *p53*$^{R175H/-}$*BACH1*$^{-/-}$ cells. Cal-33 *p53*$^{R175H/-}$*BACH1*$^{-/-}$ cells were transfected with LSD2, LSD2 + BACH1, LSD2 + BACH1Δ466-515, LSD2 + BACH1 + p53$^{R175H}$, or LSD2 + BACH1Δ466-515 + p53$^{R175H}$ plasmids and then cells lysates were ChIPed with LSD2 antibody, followed by qPCR analysis of the recruitment of LSD2 to SLC7A11 promoter. n = 3 technical replicates. The experiment was repeated twice with similar results. **f**, Western blot analysis of SLC7A11 expression in TOV-112D cells transfected with NC, p53, or LSD2 siRNAs for 48 h. The experiment was repeated twice with similar results. **g**, ChIP analysis of the recruitment of LSD2 to CEMIP promoter (-2036 to -2022) in Cal-33 native cells treated with NC, BACH1, or p53 siRNA for 48 h. n = 3 technical replicates. The experiment was repeated twice with similar results. **h**, ChIP analysis with LSD2 antibody in Cal-33 *p53*$^{R175H/-}$*BACH1*$^{-/-}$ cells. Cal-33 *p53*$^{R175H/-}$*BACH1*$^{-/-}$ cells were transfected with LSD2, LSD2 + BACH1, LSD2 + BACH1Δ466-515, LSD2 + BACH1 + p53$^{R175H}$, or LSD2 + BACH1Δ466-515 + p53$^{R175H}$ plasmids and then cells lysates were ChIPed with LSD2 antibody, followed by qPCR analysis of the recruitment of LSD2 to CEMIP promoter. n = 3 technical replicates. The experiment was repeated twice with similar results. Data represent mean of three technical replicates.
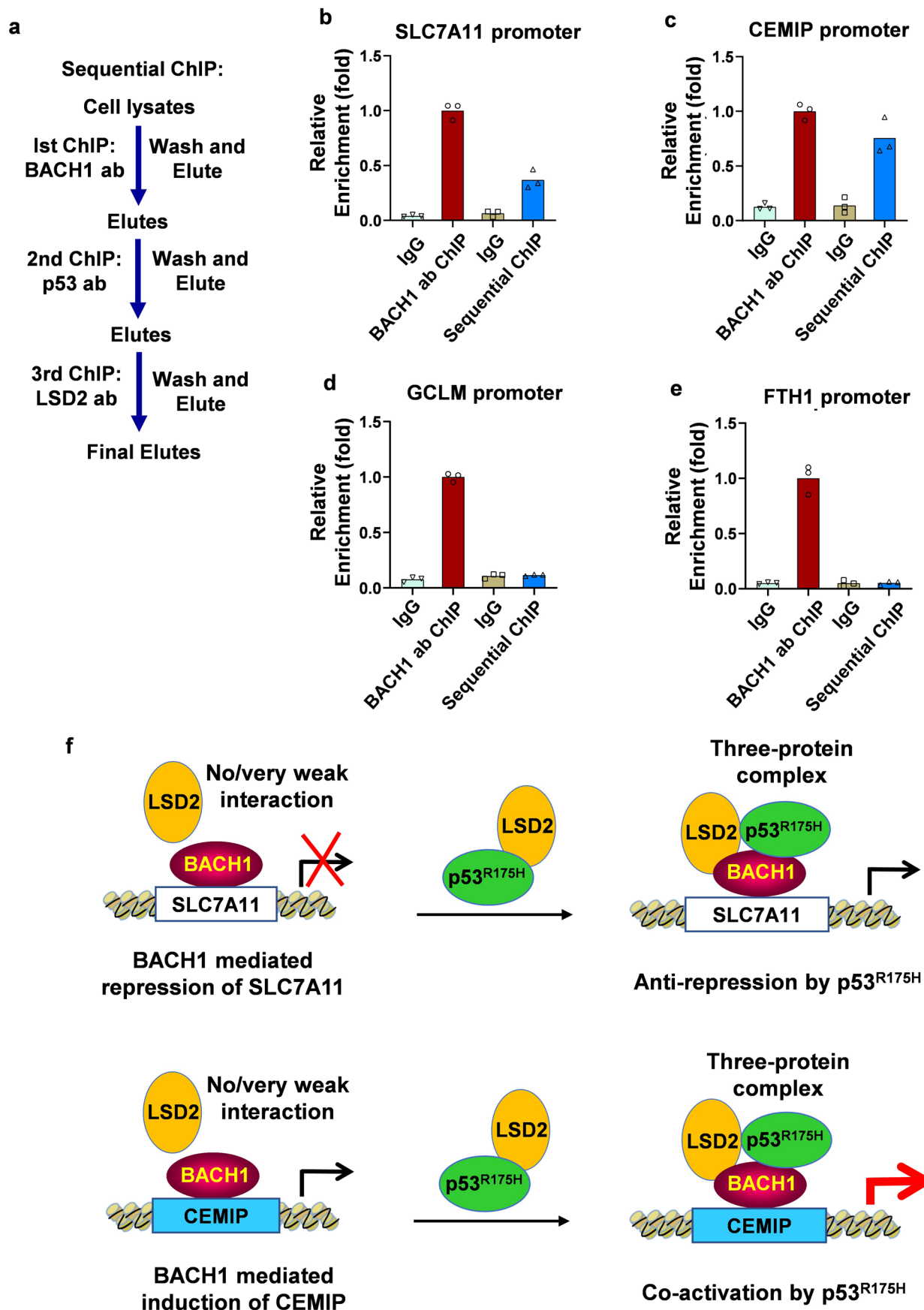
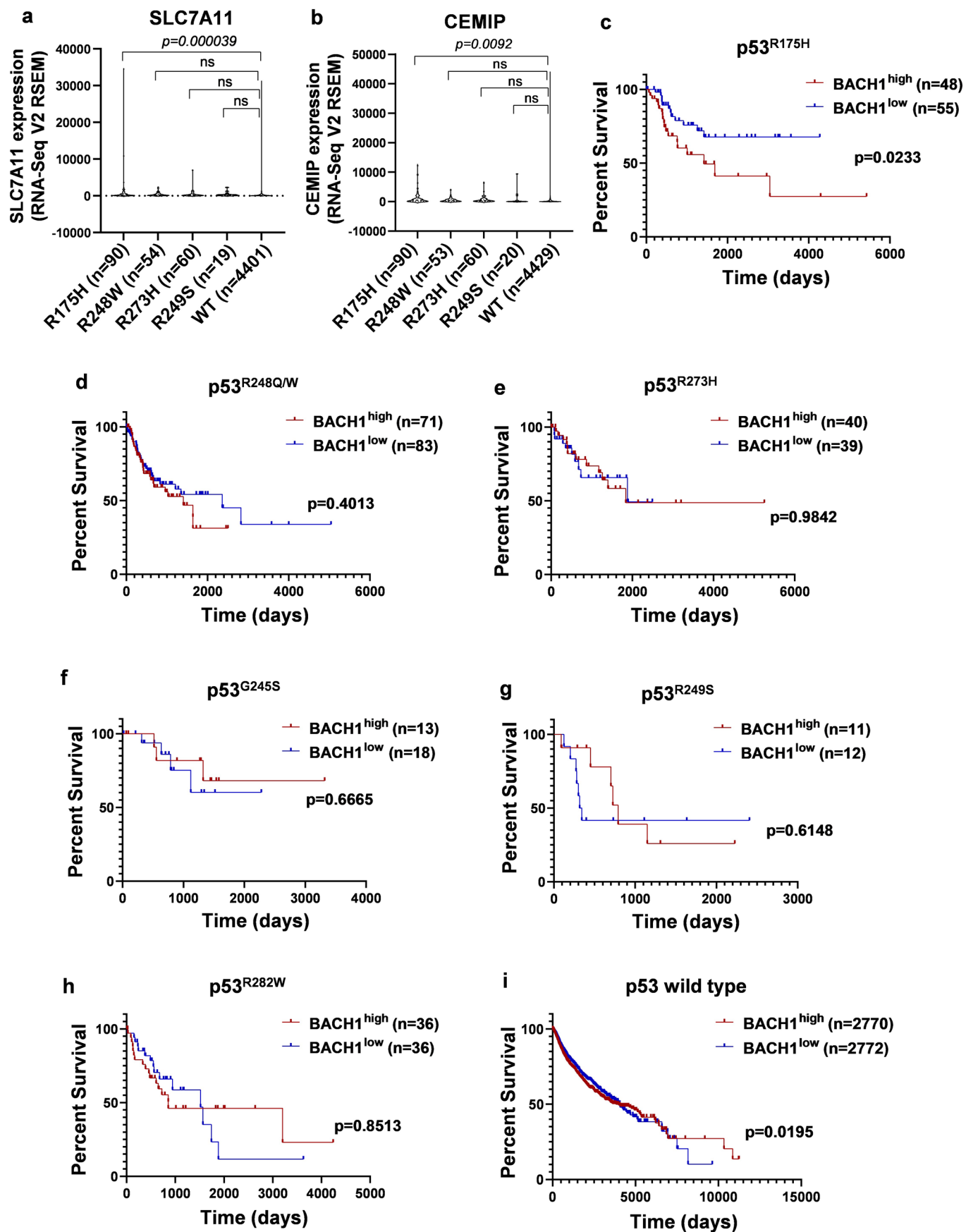**Extended Data Fig. 8 | See next page for caption.**

**Extended Data Fig. 8 | Sequential ChIP analysis of p53^R175H^-BACH1-LSD2 complex and diagram for differential regulation of repression targets and activation targets of BACH1 by p53^R175H^ and LSD2. a**, Diagram for sequential ChIP analysis. Sequential ChIP analysis was followed the established protocol by Beischlag et al 2018 (Ref. [52]). Co-enrichment of BACH1/p53^R175H^/LSD2 in gene promoter was analyzed by qPCR. **b-e**, Single ChIP assay (by BACH1 specific antibody) and sequential ChIP assay (firstly ChIP-ed by BACH1 antibody, secondly by p53 DO-1 antibody and thirdly by LSD2 antibody) for SLC7A11 promoter (**b**), CEMIP promoter (**c**), GCLM promoter (**d**) and FTH1 promoter (**e**) using Cal-33 cells. n = 3 technical replicates. The experiment was repeated twice with similar results. **f**. Diagram for differential regulation of repression targets (for example, SLC7A11) and activation targets (for example, CEMIP) of BACH1 by p53^R175H^ and LSD2. BACH1 has opposite functions in transcription on two different types of target genes: on one hand, it acts as a transcriptional repressor to downregulate a number of targets such as SLC7A11 critically involved in ferroptosis; on the other hand, BACH1 can also function as a transcriptional activator to induce pro-metastatic targets such as CEMIP to promote cancer metastasis. The interaction between LSD2 and BACH1 is very weak and unstable when p53^R175H^ is absent, but this interaction is significantly enhanced in the presence of p53^R175H^ expression since p53^R175H^ can strongly interact with both BACH1 and LSD2. p53^R175H^ is able to abrogate BACH1-mediated repression of SLC7A11 through the recruitment of LSD2 demethylase. This formation of p53^R175H^-BACH1-LSD2 complex modifies the histone methylation status at the promoter of SLC7A11 and subsequently abrogates its transcriptional repression mediated by BACH1. Conversely, the recruitment of LSD2 demethylase by p53^R175H^ to the promoter of CEMIP results in enhanced transcriptional activation of CEMIP by BACH1. Data represent mean of three technical replicates.
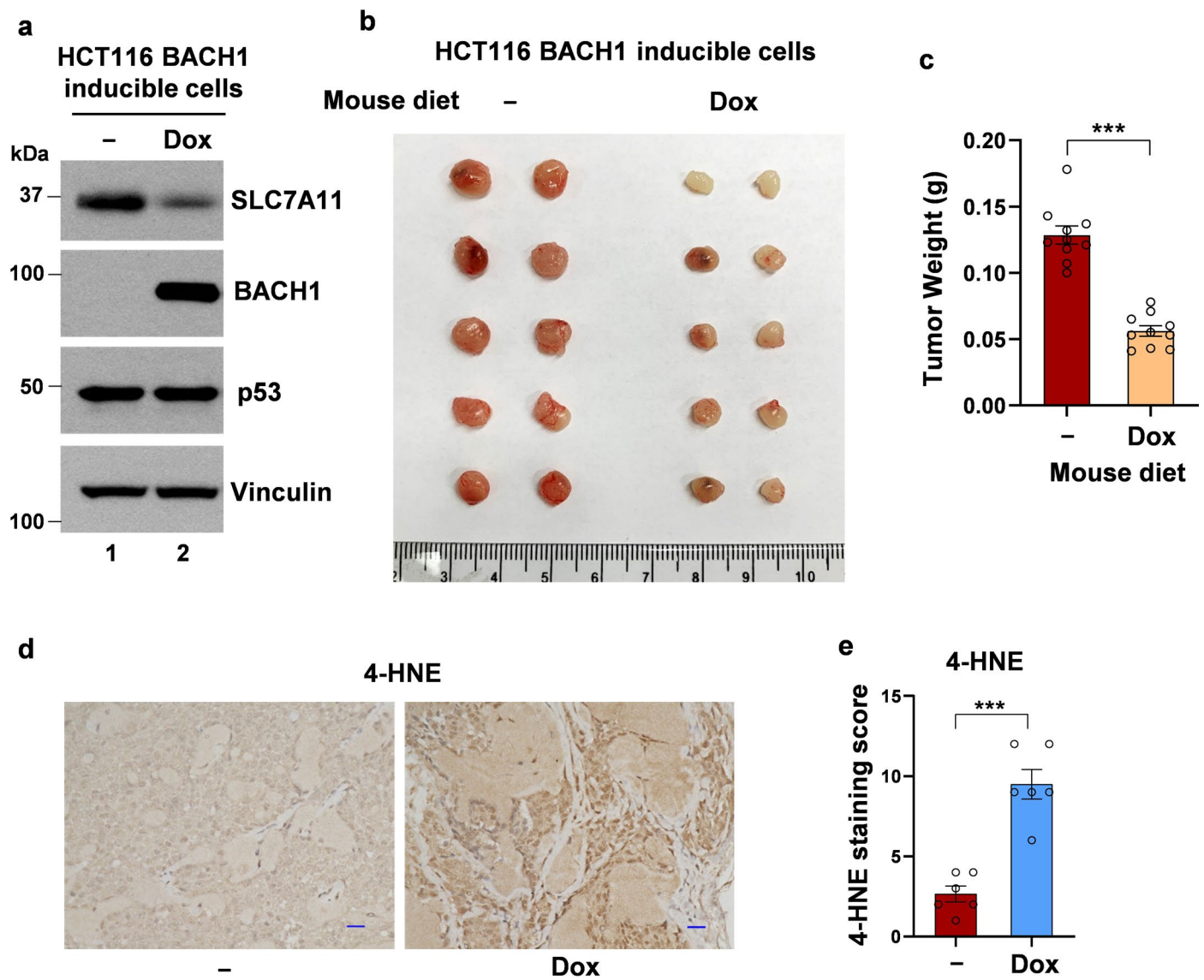
**Extended Data Fig. 9 | BACH1 suppresses tumor growth in *p53* wild-type cell line HCT116-derived xenograft tumors.** HCT116 BACH1 inducible cells were made from HCT116 *BACH1⁻ᐟ⁻* cells by transfecting BACH1 inducible plasmid. HCT116 inducible cells were pre-incubated with or without doxycycline (Dox) for 48 h in vitro and subcutaneously injected into BALB/c nude mice and mice were fed with or without doxycycline diet. **a**, Western blot analysis of SLC7A11, BACH1 and p53 expression in HCT116 BACH1 inducible cells in the presence or absence of doxycycline. The experiment was repeated three times with similar results.

**b**, Tumors isolated from nude mice implanted with HCT116 BACH1 inducible cells fed with or without doxycycline diet. Mice were sacrificed at day 20. n = 10 tumors. **c**, Tumor weights. n = 10 tumors. *P* value: <0.0001. **d**, Representative images of 4-HNE staining of HCT116 xenograft tumors. Bar scale=20μm. **e**, Quantification of 4-HNE staining using the immunoreactive score (IRS) system. n = 6 fields from 6 tumors. *P* value: <0.0001. P values were calculated by two-tailed Student's t-test. ***p < 0.001; Data represent mean + S.E.M.

**Extended Data Fig. 10 | See next page for caption.**

**Extended Data Fig. 10 | Physiological relevance of *p53* R175H mutation in cancer patients. a, b**. Violin plots of SLC7A11/ CEMIP expression in cancer patients with distinct *p53* mutation. Analyses are based on data from cBioPortal Pan-cancer studies and specific cancer types studies (271 pan-cancer and specific cancer studies were included). a, SLC7A11; b, CEMIP. *P* values were calculated by two-tailed Student's t-test. n numbers are shown on the panels. *P* values in a (from left to right): 0.000039; 0.8038; 0.6746; 0.9791. *P* values in b (from left to right): 0.0092; 0.7587; 0.916; 0.7466. **c-i**, Correlation between BACH1 expression level and patients' overall survival in different *p53* mutation status. **c**, *p53^R175H^*; **d**, *p53^R248Q/W^*; **e**, *p53^R273H^*; **f**, *p53^G245S^*; **g**, *p53^R249S^*; **h**, *p53^R282W^*; **i**, p53 wild-type. Distinct *p53* mutation patients' BACH1 expression and survival data were obtained from TCGA pan-cancer database (xenabrower.net). P values of survival curves were calculated by Log-rank (Mantel-Cox) test. n numbers are shown on the panels. *P* values: 0.0233 (c); 0.4013 (d); 0.9842 (e); 0.6665 (f); 0.6148 (g); 0.8513 (h); 0.0195 (i).

# nature portfolio

Corresponding author(s): Wei Gu

Last updated by author(s): 2-8-2023

# Reporting Summary

Nature Portfolio wishes to improve the reproducibility of the work that we publish. This form provides structure for consistency and transparency in reporting. For further information on Nature Portfolio policies, see our Editorial Policies and the Editorial Policy Checklist.

## Statistics

For all statistical analyses, confirm that the following items are present in the figure legend, table legend, main text, or Methods section.

| n/a | Confirmed | |
|---|---|---|
| ☐ | ☒ | The exact sample size (*n*) for each experimental group/condition, given as a discrete number and unit of measurement |
| ☐ | ☒ | A statement on whether measurements were taken from distinct samples or whether the same sample was measured repeatedly |
| ☐ | ☒ | The statistical test(s) used AND whether they are one- or two-sided *Only common tests should be described solely by name; describe more complex techniques in the Methods section.* |
| ☒ | ☐ | A description of all covariates tested |
| ☒ | ☐ | A description of any assumptions or corrections, such as tests of normality and adjustment for multiple comparisons |
| ☐ | ☒ | A full description of the statistical parameters including central tendency (e.g. means) or other basic estimates (e.g. regression coefficient) AND variation (e.g. standard deviation) or associated estimates of uncertainty (e.g. confidence intervals) |
| ☐ | ☒ | For null hypothesis testing, the test statistic (e.g. *F*, *t*, *r*) with confidence intervals, effect sizes, degrees of freedom and *P* value noted *Give P values as exact values whenever suitable.* |
| ☒ | ☐ | For Bayesian analysis, information on the choice of priors and Markov chain Monte Carlo settings |
| ☒ | ☐ | For hierarchical and complex designs, identification of the appropriate level for tests and full reporting of outcomes |
| ☒ | ☐ | Estimates of effect sizes (e.g. Cohen's *d*, Pearson's *r*), indicating how they were calculated |

*Our web collection on statistics for biologists contains articles on many of the points above.*

## Software and code

Policy information about availability of computer code

| Data collection | FACS data were acquired with Attune NxT Acoustic Focusing Cytometer; Metastasis images were acquired with KEYENCE BZ-X800 fluorescence microscope; Cell death data and dual-luciferase assay data were collected using GloMax® Explorer Multimode Microplate Reader (Promega). Quantitative PCR data were collected using 7500 Fast Real-Time PCR System (Applied Biosystems); In vivo luminescence images were acquired with IVIS Spectrum Optical Imaging System. |
|---|---|
| Data analysis | Statistical analyses were done with Excel V2016 and GraphPad Prism V9; FACS data were analyzed with FlowJo Version 10; Lung metastases were quantified by KEYENCE BZ-X800 Analyzer. |

For manuscripts utilizing custom algorithms or software that are central to the research but not yet described in published literature, software must be made available to editors and reviewers. We strongly encourage code deposition in a community repository (e.g. GitHub). See the Nature Portfolio guidelines for submitting code & software for further information.

## Data

Policy information about availability of data

All manuscripts must include a data availability statement. This statement should provide the following information, where applicable:

- Accession codes, unique identifiers, or web links for publicly available datasets
- A description of any restrictions on data availability
- For clinical datasets or third party data, please ensure that the statement adheres to our policy

RNA-sequencing data from Cal-33 cells have been deposited to the Gene Expression Omnibus under accession code GSE224730. An analyzed result for this RNA-sequencing is available in Supplementary Table 1. Proteomics data have been deposited in ProteomeXchange via the PRIDE database, with a relevant accession number PXD039886. The human pancancer data were derived from the TCGA Research Network: http://cancergenome.nih.gov/ and cBioPortal: https://www.cbioportal.org/. The data-set derived from this resource that supports the findings of this study is available in Source Data Extended Data Fig.10. Source data for Fig. 1-8 and Extended Data Fig. 1-10 have been provided as Source Data files. All other data supporting the findings of this study are available from the corresponding author on reasonable request.

## Human research participants

Policy information about studies involving human research participants and Sex and Gender in Research.

| | |
|---|---|
| Reporting on sex and gender | N/A |
| Population characteristics | N/A |
| Recruitment | N/A |
| Ethics oversight | N/A |

Note that full information on the approval of the study protocol must also be provided in the manuscript.

# Field-specific reporting

Please select the one below that is the best fit for your research. If you are not sure, read the appropriate sections before making your selection.

☒ Life sciences ☐ Behavioural & social sciences ☐ Ecological, evolutionary & environmental sciences

For a reference copy of the document with all sections, see nature.com/documents/nr-reporting-summary-flat.pdf

# Life sciences study design

All studies must disclose on these points even when the disclosure is negative.

| | |
|---|---|
| Sample size | No statistical method was used to predetermine sample size. For in vivo experiments, we used at least 5 mice per group which is sufficient to detect meaningful biological difference. For in vitro experiments, unless otherwise stated, n=3 was chosen as the number of sample size. Sample size n=3 is sufficient for in vitro experiment as the variability between samples from in vitro experiments is low. |
| Data exclusions | No data was excluded from this study. |
| Replication | All experiments were repeated independently at least two or three times with similar results, and representative results are shown. |
| Randomization | Nude mice used for xenograft and metastasis experiments were randomly allocated into each experimental group. In vitro experiments were not randomized; all samples were analyzed equally without sub-sampling, therefore, there was no need for randomization. |
| Blinding | For cell-based in vitro experiments, the investigators were not blinded on data acquisition and analysis. For animal studies, the investigators were not blinded to the experimental group allocation. Blinding was not used in any experiment in this study since it is not possible based on treatment and general conditions of the samples used. |

# Reporting for specific materials, systems and methods

We require information from authors about some types of materials, experimental systems and methods used in many studies. Here, indicate whether each material, system or method listed is relevant to your study. If you are not sure if a list item applies to your research, read the appropriate section before selecting a response.

## Materials & experimental systems

| n/a | Involved in the study |
|---|---|
| ☐ | ☒ Antibodies |
| ☐ | ☒ Eukaryotic cell lines |
| ☒ | ☐ Palaeontology and archaeology |
| ☐ | ☒ Animals and other organisms |
| ☒ | ☐ Clinical data |
| ☒ | ☐ Dual use research of concern |

## Methods

| n/a | Involved in the study |
|---|---|
| ☒ | ☐ ChIP-seq |
| ☐ | ☒ Flow cytometry |
| ☒ | ☐ MRI-based neuroimaging |

## Antibodies

**Antibodies used**

BACH1 (clone F9) (WB, 1:1000)  Santa Cruz Biotechnology  Cat#sc-271211
BACH1 (WB, 1:1000; IP, 1:250)  Bethyl Laboratories  Cat#A303-058A
BACH1 (ChIP, 4µg/1 ml cell lysate) R and D Systems  Cat#AF5776
H3K4me2 (ChIP, 1:200)  Millipore  Cat#07-030
p53 (FL-393) (WB, 1:1000; ChIP, 1:250)  Bioss Antibodies  Cat#bs-8687R
p53 (clone DO-1) (IP, 1:50; WB, 1:1000; ChIP, 1:50)  Santa Cruz Biotechnology  Cat#sc-126
p53 (CM5) (WB, 1:1000; IP, 1:250)  Leica Biosystems  Cat#NCL-L-p53-CM5p
Flag (clone M1) (WB, 1:1000)  Sigma Cat#F3040
HA (clone 3F10) (WB, 1:1000)  Sigma Cat#11867423001
Vinculin (clone hVIN-1) (WB, 1:3000)  Sigma Cat#V9131
SLC7A11  (clone D2M7A) (WB, 1:1000)  Cell Signaling Cat#12691
CEMIP (WB, 1:3000, suitable for human)  Novus Biologicals  Cat#45750002
CEMIP (WB, 1:3000, suitable for mouse)  Novus Biologicals  Cat#NBP1-58029
β-actin (WB, 1:2000)  Abcam  Cat#ab8227
ACSL4 (clone A-5) (WB, 1:1000) Santa Cruz Biotechnology  Cat#sc-271800
LSD2 (clone EPR18508) (WB, 1:1000)  Abcam  Cat#ab193080
Ki67 (clone SP6) (IHC, 1:200)  Abcam  Cat#ab16667
4-HNE (IHC, 1:200)  Abcam  Cat#ab46545
Normal rabbit IgG (IP/ChIP, 4µg/1ml cell lysate)  Santa Cruz Biotechnology  Cat#sc-2027
Normal goat IgG (ChIP, 4µg/1 ml cell lysate)  R&D  Cat#AB-108-C
Normal mouse IgG (IP, 4µg/1 ml cell lysate)  Santa Cruz Biotechnology  Cat#sc-2025
HRP-conjugated anti-mouse (WB, 1:10000) SouthernBiotech  Cat#1031-05
HRP-conjugated anti-rabbit (WB, 1:10000)  SouthernBiotech  Cat#4050-05
HRP-conjugated anti-rat (WB, 1:10000) SouthernBiotech  Cat#3050-05

**Validation**

All antibodies used in this study are commercially available and have been validated by manufacturer. Antibody validation and validation criteria are available on the following websites:
BACH1 (WB) https://www.scbt.com/zh/p/bach1-antibody-f-9
BACH1 (WB and IP) https://www.fortislife.com/products/primary-antibodies/rabbit-anti-bach1-antibody/BETHYL-A303-058
BACH1 (ChIP) https://www.rndsystems.com/cn/products/human-bach1-antibody_af5776
H3K4me2 antibody https://www.emdmillipore.com/US/en/product/Anti-dimethyl-Histone-H3-Lys4-Antibody,MM_NF-07-030
p53 (FL-393)  https://www.biossusa.com/products/bs-8687r
p53 (DO-1) (IP and WB) https://www.scbt.com/p/p53-antibody-do-1
p53 (CM5) (WB and IP) https://shop.leicabiosystems.com/us/ihc-ish/ihc-primary-antibodies/pid-p53-protein-cm5
Flag https://www.sigmaaldrich.com/catalog/product/sigma/f3040?lang=en&region=US
HA https://www.sigmaaldrich.com/US/en/product/roche/roahaha?
gclid=Cj0KCQiA8lCOBhDmARIsAEGI6o2QUUxB0qMoKX683PHl8ha6Ho57Ziic5CgGAkvgDP1In8yE874l-DQaAhOnEALw_wcB
Vinculin https://www.sigmaaldrich.com/catalog/product/sigma/v9131?lang=en&region=US&cm_sp=Insite-_-
caSrpResults_srpRecs_srpModel_v9131-_-srpRecs3-1
SLC7A11 https://www.cellsignal.com/products/primary-antibodies/xct-slc7a11-d2m7a-rabbit-mab/12691
CEMIP (for human) https://www.novusbio.com/products/cemip-kiaa1199-antibody_45750002
CEMIP (for mouse) https://www.novusbio.com/products/cemip-kiaa1199-antibody_nbp1-58029
β-actin https://www.abcam.com/beta-actin-antibody-ab8227.html
LSD2 https://www.abcam.com/lsd2--aof1-antibody-epr18508-ab193080.html
ACSL4 https://www.scbt.com/p/acsl4-antibody-a-5
Ki67 https://www.abcam.com/ki67-antibody-sp6-ab16667.html
4-HNE https://www.abcam.com/4-hydroxynonenal-antibody-ab46545.html?productWallTab=Abreviews
Normal rabbit IgG (IP/ChIP) https://datasheets.scbt.com/sc-2027.pdf
Normal goat IgG (ChIP) https://www.rndsystems.com/cn/products/normal-goat-igg-control_ab-108-c
Normal mouse IgG (IP), https://www.scbt.com/zh/p/normal-mouse-igg
HRP-conjugated anti-mouse https://www.southernbiotech.com/?catno=1031-05&type=Polyclonal#&panel1-1&panel2-1
HRP-conjugated anti-rabbit https://www.southernbiotech.com/?catno=4050-05&type=Polyclonal#&panel1-1&panel2-1
HRP-conjugated anti-rat https://www.southernbiotech.com/?catno=3050-05&type=Polyclonal#&panel1-1&panel2-1

# Eukaryotic cell lines

Policy information about cell lines and Sex and Gender in Research

| | |
|---|---|
| Cell line source(s) | KLE, 293T, H1299, HCT116, U2OS, TOV-112D, T-47D, BT-549, BT-474, MDA-MB-468, MDA-MB-231, and HCC1937 cells were purchased from the American Type Culture Collection (ATCC). Cal-33 cells and HuCCT1 cells were purchased from Creative Bioarray (Shirley, NY). p53R172H/R172H mice derived sarcoma cells were made in our lab. |
| Authentication | All cell lines were not authenticated. |
| Mycoplasma contamination | The cell lines were tested negative for mycoplasma contamination. |
| Commonly misidentified lines (See ICLAC register) | No cell line used in the study was found in the databases of commonly misidentified cell lines that are maintained by ICLAC and NCBI biosample. |

# Animals and other research organisms

Policy information about studies involving animals; ARRIVE guidelines recommended for reporting animal research, and Sex and Gender in Research

| | |
|---|---|
| Laboratory animals | Balb/c NU/NU nude mice (CAnN.Cg-Foxn1nu/Crl, female, 6-week-old) were purchased from Charles River Laboratories for xenograft and metastasis experiments; p53R172/+ mice (129S4/SvJae, male, 8-week-old) were from Dr. Kenneth P. Olive's lab; BACH1-/- mice (female, 8-week-old, C57BL/6J) were from Dr. Kazuhiko Igarashi's lab; Wildtype C57BL/6J mice (#:000664, female, 8-week-old) were from the Jackson Laboratory. |
| Wild animals | The study did not use any wild animal. |
| Reporting on sex | For nude mice-related xenograft and metastasis experiments, we used female mice for the reason that it can reduce fighting behavior, but our study was not focused on sex-associated outcomes/phenotypes/mechanisms. In p53R172/+ mice and p53R172/+BACH1-/- mice metastasis experiment, we included mice with both sexes. |
| Field-collected samples | No field-collected sample was used in the study. |
| Ethics oversight | The study is compliant with all the relevant ethical regulations for animal experiments. All experimental protocols were approved by the Institutional Animal Care and Use Committee of Columbia University . If the tumor size/burden exceeds 1.5cm in diameter, the mice will be euthanized. We confirm that the maximal tumour size/burden was not exceeded in this study. |

Note that full information on the approval of the study protocol must also be provided in the manuscript.

# Flow Cytometry

## Plots

Confirm that:

☒ The axis labels state the marker and fluorochrome used (e.g. CD4-FITC).

☒ The axis scales are clearly visible. Include numbers along axes only for bottom left plot of group (a 'group' is an analysis of identical markers).

☒ All plots are contour plots with outliers or pseudocolor plots.

☒ A numerical value for number of cells or percentage (with statistics) is provided.

## Methodology

| | |
|---|---|
| Sample preparation | For in-vitro cultured cells staining, cells were treated with TBH for indicated time and incubated with BODIPY™ 581/591 C11 (Thermo Fisher Scientific, Cat#D3861) at the concentration of 2.5 μM for 25-30 min at 37 degree in serum-free medium, and then cells were washed with PBS, digested, and washed with PBS again, followed by FACS analysis of lipid peroxidation level. For tumor-derived cells staining, fresh tumor tissues were sliced and cut into small pieces, and digested with 1 mg/ml collagenase, Type I (Thermo Fisher Scientific, Cat#17018029) for 1 h at 37 degree, and then tissues were pipetted and filtered through syringe needles to obtain single cells. Cells were subjected to BODIPY™ 581/591 C11 staining for 25-30 min at RT in a rotator, followed by FACS analysis of lipid peroxidation level. |
| Instrument | Attune NxT Acoustic Focusing Cytometer |
| Software | FlowJo Version 10 |
| Cell population abundance | 10, 000 gated cells were analyzed for each sample. |
| Gating strategy | Viable cells were identified by using FSC-A/SSC-A gating; Singlet cells were identified by using FSC-A/FSC-H gating. |

☒ Tick this box to confirm that a figure exemplifying the gating strategy is provided in the Supplementary Information.